Electrical resistivity tomography results analyzed with two inversion methods to determine chloride profiles on BFS concrete having very high electrical resistivity

Mohamad Khodor El Achrafi, Stéphanie Bonnet, Géraldine Villain

ERT results analyzed with two inversion methods to determine chloride profiles on BFS concrete having very high electrical resistivity

Mohamad Khodor EL ACHRAFI[1,2], Stéphanie BONNET[1], Géraldine VILLAIN[2]

[1] Nantes University, Ecole Centrale Nantes, CNRS, GeM, UMR 6183 F-44600 Saint-Nazaire France
mohamad.el-achrafi@univ-nantes.fr, stephanie.bonnet@univ-nantes.fr
[2] Univ Gustave Eiffel, MAST-LAMES, Campus de Nantes, Allée des Ponts et Chaussées, CS5004, F-44344 Bouguenais, France
geraldine.villain@univ-eiffel.fr

Abstract: Non-destructive evaluation techniques are increasingly used for the investigation of reinforced concrete structures in marine environment. In this paper, the possibility of evaluating chloride profiles by Electrical Resistivity Tomography (ERT) on Blast furnace slag (BFS) concrete at a long curing period so having high electrical resistivity was studied. This was carried out by monitoring the chloride profile for two 6-years old concretes (with and without slag) during a diffusion campaign using a Non-Destructive Evaluation (NDE) methodology. The methodology is based on determining the electrical resistivity profiles by carrying out surface apparent resistivity measurements submitted to two different inversion processes. The resistivity profiles are then converted to chlorides profiles using calibration curves. The chlorides profiles were also compared by those assessed by Destructive Evaluation (DE) at three different exposure periods, which displays a high similarity between DE and NDE profiles.

Keywords: Slag, electrical resistivity, chloride ingress, durability indicators, curing.

1. Introduction

Considering the severe exposure conditions in the marine environment and the wide consumption of de-icing salts in cold countries, chloride ingress in concrete leading to the corrosion of steel is one of the most common pathologies of reinforced concrete structures. Depending on which exposure conditions concrete structure is submitted [1], chloride ions can penetrate into concrete through multiple mechanisms such as diffusion, adsorption or convection. In this work, the saturated exposure zone was studied where chlorides penetrate into concrete through diffusion under a concentration gradient [2,3].

Tuutti (1982) [4] suggested that the corrosion process for reinforcing structures passes into three deterioration phases from chloride penetration until reinforcement steel corrosion. The first one known as ‘incubation phase’ corresponds to the phase when chlorides are located in the cover concrete. The second one called the ‘initiation phase’, when chlorides depassivate the reinforcement steel surface, leads to the beginning of corrosion. The last phase is the ‘propagation phase’ during which the corrosion develops and cracks start appearing in concrete.

In the incubation phase, concrete cover plays a crucial role by protecting reinforcing steel from corrosion. This protection is ensured by delaying the chloride ions ingress until reaching the critical-corrosion concentration at the level of the reinforcing bars [5]. Therefore, different strategies were proposed to slow down chloride penetration and stay in the incubation phase. One of these methods consists in modifying the cementitious matrix via the incorporation of Supplementary Cementitious Materials (SCMs) [6–10].

The incorporation of SCMs can be realized with partial substitution of Portland Cement (PC), cement usually used in the typical concrete mix, by an alternative cementitious addition as Blast Furnace Slag (BFS). The latter is one of the most SCMs used to increase the chloride resistance of the concrete by modifying the Durability Indicators (DIs) [7,11–13]. A considerable amount of research have shown the slag effect on concrete-chloride resistance by assessing the apparent diffusion coefficient $D_{a(mig)}$ [6,14,15]. All these studies showed an important reducing in the chloride diffusivity of concrete when BFS was incorporated with different percentages.

Indeed, the majority of laboratory studies or on site evaluation to determine chloride content in BFS concrete were carried out by the Destructive Evaluation (**DE**) method [12,16–19]. This type of method is known to be very exhausting, time-consuming and harmful for the structure. As well as, it is impossible to monitor the evolution of chloride content in the same position, due to the fact that the concrete is destroyed by grinding. Therefore, it was very important to develop a Non-Destructive Evaluation (**NDE**) methodology to get the chloride profiles for high incorporation of slag.

One of the most sensitive NDE methods to the ionic content in concrete is the electromagnetic techniques and the DC/AC applied current technique. Several research studies had proved the sensitivity of these techniques to the chloride content in concrete with Portland cement which presents low resistivity compared to BFS concrete [20–25]. Among the existing electromagnetic and DC/AC applied current technique techniques, this paper focuses on the Direct Current (DC) electrical resistivity method with Wenner configuration [22,26–29].

Indeed, several researches studied the effect of slag on the electrical resistivity of concrete [6,30,15,31–33] but mainly with the Wenner four-probe system which gives a global resistivity measurement. Divsholi et al. (2014) [30] quantified the effect of 50% of cement replacement with BFS on the global electrical resistivity of concrete at different water-to-binder ratios (w/b = 0.4, 0.5 and 0.6). The electrical resistivities for concretes with 50% of BFS were 720, 500, and 330 Ω.m for w/b=0.4, 0.5 and 0.6, respectively. Whereas the electrical resistivities for

concrete without BFS incorporation exhibit a lower value: 220, 180 and 110 Ω.m for w/b=0.4, 0.5 and 0.6, respectively. Elahi et al. (2010) [31] and Teng et al. (2013) [15] explained this increasing in the electrical resistivity by the densification of the microstructure due to the pozzolanic reaction of the slag, which results in the formation of secondary C-S-H hydrates. Lübeck et al. (2012) [32] observed also an increase in the concrete's electrical resistivity and a reduction in the electrical conductivity of the pore solution by the substitution of PC by BFS.

It's worth mentioning herein that all the works that exist in the literature concerning the effect of slag incorporation on concrete properties as resistivity were carried out at a **short curing periods** (between 28 and 90 days). Additionally, only the global electrical resistivity was predicted in the literature; a resistivity profile as a function of concrete depth and a subsequent chloride profile were not found.

For this study, the Electrical Resistivity Tomography (ERT) device developed by Du Plooy et al. (2013) [34] to get concrete properties on Portland concrete was used to measure the apparent electrical resistivity on concrete with and without BFS exposed to salted solution. Indeed, the apparent values of the measurements obtained using the ERT method rely on the geometry and electrode configuration used, and as a result, on the investigation volume of the measurements. Therefore, the measurements are inverted to estimate the electric resistivity profile in concrete. However, the resistivity profiles exhibited in the literature for ordinary concretes were, in fact, determined solely using Res1d software, making them presented as non-continuous layer. Thus, the application of a new inversion method (CERIS) that uses continuous parameterizations based on actual resistivity profile shapes is presented in this study.

Moreover, given the difficulty of injecting an electrical current due to BFS concrete's extremely high resistivity, determining a resistivity profile using ERT will be quite challenging. The aim of this work is to know if this technique will be valid for quite mature BFS concrete with very high electrical resistivity. Once this NDE methodology will be validated on laboratory specimens, it could be then used to auscultate in-situ structures. However, the reinforcements presented in field structure affect the apparent resistivity measurement specifically for those obtained near to the rebar reinforcement [35]. Nevertheless, the study of Alhajj et al., 2019 [36] showed that the presence of the reinforcements only disturbs the apparent resistivity and not the 'real' resistivity profile of the concrete. Therefore, an improvement of the apparent resistivity inversion method has been developed leading to obtain the "real" resistivity distribution despite the presence of reinforcements provided that their characteristics are taken into consideration. (position, geometry, electrical properties and contact with the concrete).

So, this paper aims to investigate the use of ERT technique described in section 2 for monitoring the chloride content profiles evolution, for two concretes C1 (without BFS) and C3 (with BFS) at 11 different exposure periods during a diffusion campaign as depicted in section 3. In section 4, the effect of curing period was studied by comparing the concrete properties and microstructures obtained at 90 days and 6 years of curing. Furthermore, the evolution of the concrete electrical resistivity was related and used to calculate the NDE chloride profiles which will be compared with the DE chloride profiles at three different exposure periods (12, 19 and 46 weeks). This paper ends with some concluding remarks presented in section 5.

2. NDE methodology for the determination of the chloride profiles

2.1. Measurement principle with ERT device

The ERT device which was employed in previous works to monitor the chloride penetration into Portland concrete [18, 35] was used in this paper to determine the apparent electrical resistivity of concrete slabs submitted to chloride diffusion. It is composed of a multi-electrode resistivity probe (fourteen hollow metallic electrodes) aligned and equally spaced (2 cm). The electrodes are filled with wetted sponges in order to enhance the electrical current injection by reducing contact resistance (see Figure 1.a).

The Wenner configuration [38] was chosen in this study to measure the electrical resistance R (Ohm symbolized by Ω) due to its high sensitivity variation with depth [26]. It is based on measuring the potential drop U (V) between the internal electrodes due to the injection of an electrical current I (A) throughout two external electrodes. The measurement sequence for the Wenner configuration was programmed on a commercial resistivity meter (Syscal Pro, Iris Instruments®). Once the current intensity and the potential drop were obtained, the electrical resistance R (Ω) can be determined using Ohm's law ($R=U/I$).

Notice that the electrical resistance R is multiplied by a geometric factor G_R (m) in order to obtain the apparent resistivity ρ_a (Ω.m). Based on the studies of Marescot et al. (2006) [39], the geometric factor was computed by numerical modeling with a finite element software (COMSOL Multiphysics®) using AC/DC module and by taking into account the slab geometry and the electrodes configuration [39,34,29,40].

As Wenner configuration was applied to the fourteen electrodes, four different electrodes spacings (a = 2, 4, 6 and 8 cm) were possible. Consequently, four investigation depths could be obtained denoted as 'Level 1, Level 2, Level 3 and Level 4' (see Figure 1.b).

In this work, three set of measurements were realized at each level: one in the middle of the slab and two others 10 mm apart from both side of the middle measurement (see Figure 1.a). The measurements were realized by leaving 3 cm between the edge and the electrodes at the ends, in order to avoid as much as possible the edge effects [41]. For each measurement, the number of measured apparent resistivities are 11, 8, 5 and 2 for level 1, 2, 3 and 4, respectively. The average of the three sets of measurement were calculated for each level and thus four apparent resistivity were determined (one apparent resistivity per level denoted as $\rho_{a1}, \rho_{a2}, \rho_{a3}$ and ρ_{a4}). In order to determine the "real resistivity" as function of depth, i.e. resistivity profiles, an inversion process is necessary and is detailed in §2.2.

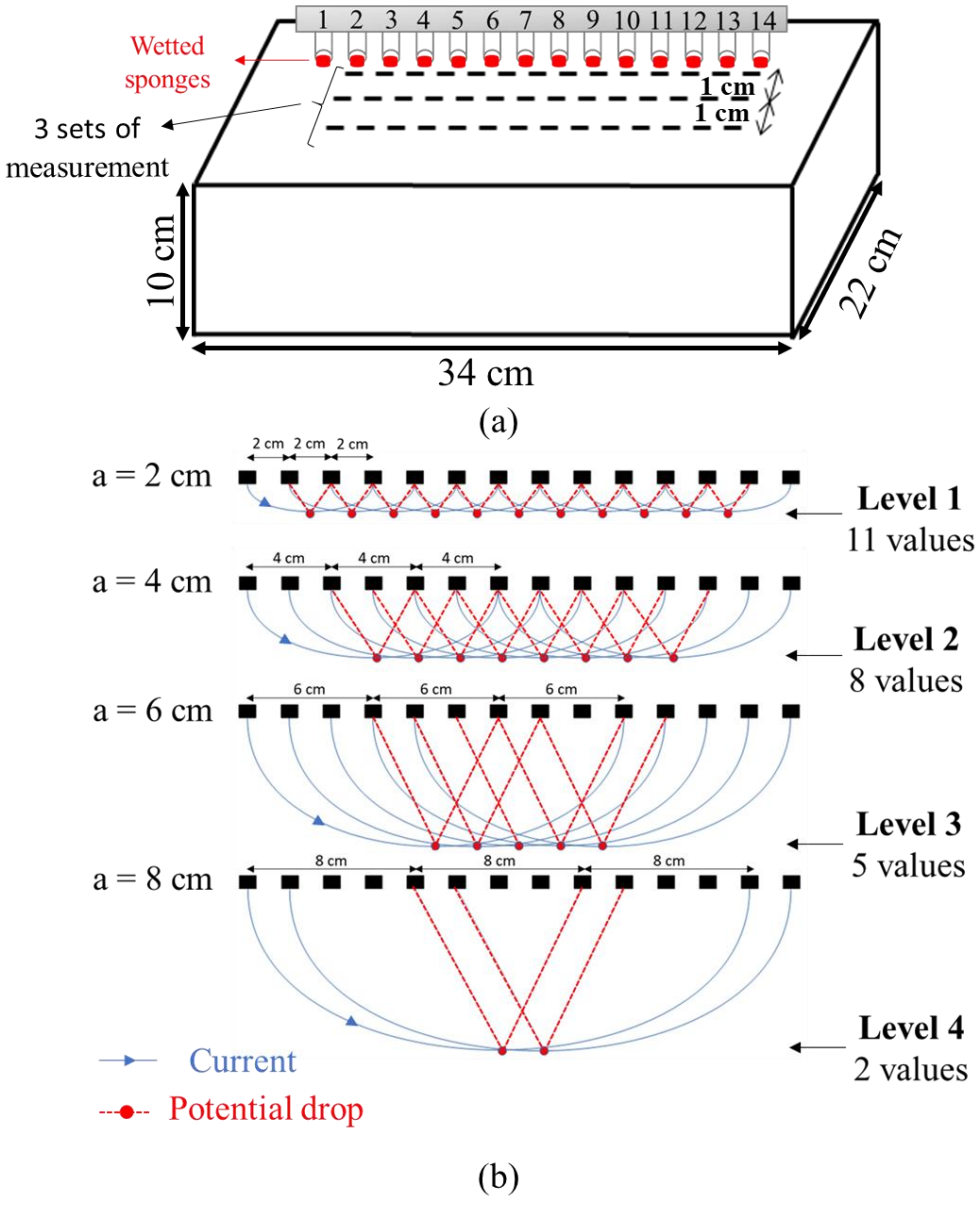

Figure 1: Scheme describing the ERT device measurements: (a) electrodes position on the slab and measurements position, (b) investigation levels and number of apparent resistivity

2.2. NDE methodology to obtain chloride profiles using ERT device

The methodology used to determine chloride profiles using ERT device is based on **three Steps** described in Figure 2.

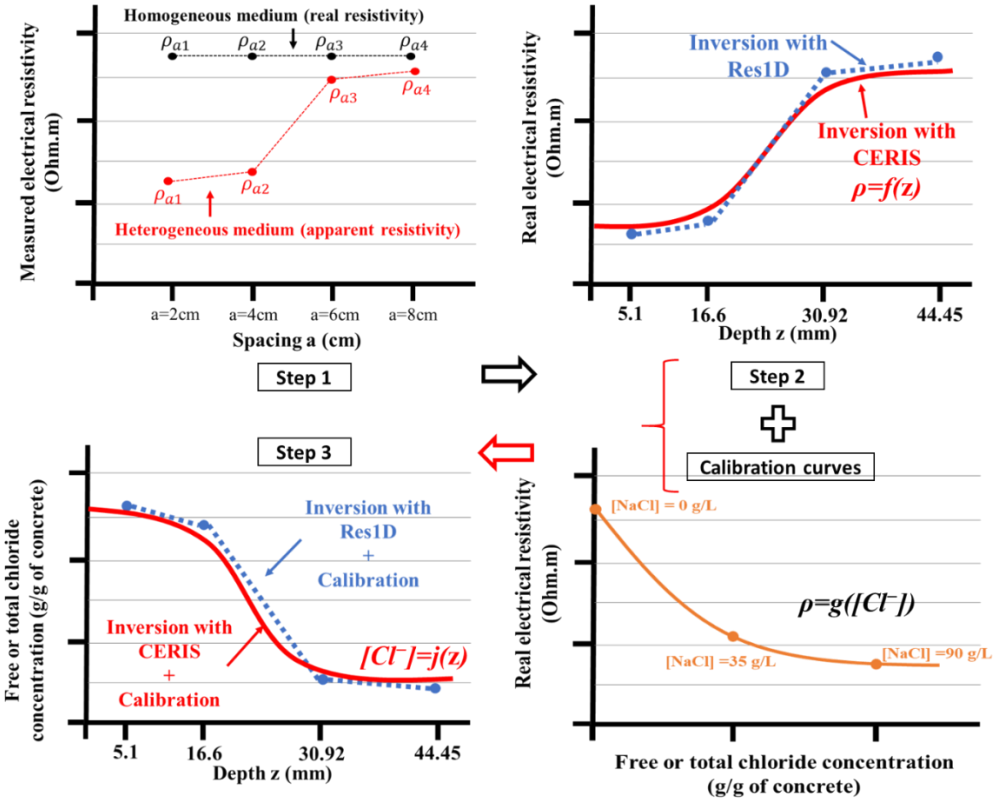

Figure 2: Followed steps used to obtain free or total chlorides profile using ERT device

2.2.1.Apparent resistivity measurements: step 1

In **Step 1**, the apparent resistivity is obtained after carrying out ERT measurements following the procedure mentioned previously. It's worth mentioning herein, that for a homogeneous concrete (including homogeneous hydric or ionic conditions), the resistivity is the same over the entire homogeneous medium. Thus, the apparent resistivity is equal to the real resistivity of the concrete being tested [26]. In the case of concrete with heterogeneous hydric or ionic conditions along depth, the apparent resistivity varies.

2.2.2.Resistivity profiles: step 2

As mentioned previously, each apparent resistivity represents an integrated value over a volume related to electrodes spacing. Consequently, the **Step 2** aims to invert the apparent resistivities in order to estimate the real resistivity profile in concrete using two different methods. The first one was carried out using the free Res1D software [42]. Four resistivities values were

determined by Res1D related to four layers with different thicknesses (10.2, 12.75, 15.94 and 11.86 mm) and then they were displayed at the center of each layer (5.1, 16.57, 30.92 and 44.45 mm) (see **step 2** in Figure 2). Then, the limit depth beyond which we can no longer see the effect of chlorides on resistivity is 50 mm. However, having a limited number of resistivity layer (only 4), can affect negatively the inverted results and then the resistivity and chloride profile.

Thus, a second inversion method called CERIS developed to get moisture profiles [29,40] was carried out using an optimized model parameterization in order to use a continuous function based on a realistic resistivity profile shape. Before explain the inversion procedure, it should be mentioned that CERIS method defines the resistivity profile to be adequately adjusted with the following Weibull curve expression:

$$\rho(z) = (\Theta_1 - \Theta_2).exp.\left(-\left(\frac{z}{\Theta_3}\right)^{\Theta_4}\right) + \Theta_2 \quad (1)$$

where z is the depth in concrete slab (m), Θ_1 is the resistivity of concrete at the surface (Ω), Θ_2 is the asymptotic resistivity at infinite depth (Ω), Θ_3 and Θ_4 are the scale parameter of the curve (m) and is the shape parameter of the curve, respectively.

CERIS method is based on minimizing the following least-squares misfit criterion:

$$\psi(\Theta) = \sum_{i=1}^{n} \left(\rho_{a,i\ mod}(\Theta) - \rho_{a,i\ mes}\right)^2 \quad (2)$$

where $\rho_{a,mod}(\Theta)$ is the vector collecting each simulated resistivity $\rho_{a,i\,mod}(\Theta)$ for a given set of profile parameters in vector $\Theta = [\Theta_1,\Theta_2,\Theta_3,\Theta_4]$ and $\rho_{a,mes}$ similarly collects the measured resistivity. The Levenberg-Marquardt nonlinear least-squares procedure is used to minimize the function ψ [43,44].

The inversion scheme is explained in Figure 3. It is an iterative process which starts with an initial resistivity profile given by initial parameter $\Theta^{(0)}$. Then, the initial apparent resistivities $\rho_{a,mod}{}^{(0)}$ were computed by solving the forward problem using COMSOL Multiphysics® module AC/DC Electric Currents [40,45]. The initial modelled apparent resistivities $\rho_{a,mod}{}^{(0)}$ are then minimized according to the measured apparent resistivities $\rho_{a,mes}$ so the criterion $\psi(\Theta^{(0)})$ is computed. Initial parameters are then updated until fulfilling the stopping criteria explained in [40]. Finally, the four optimal parameters are computed Θ and the continuous resistivity profile is obtained which is called CERIS profile.

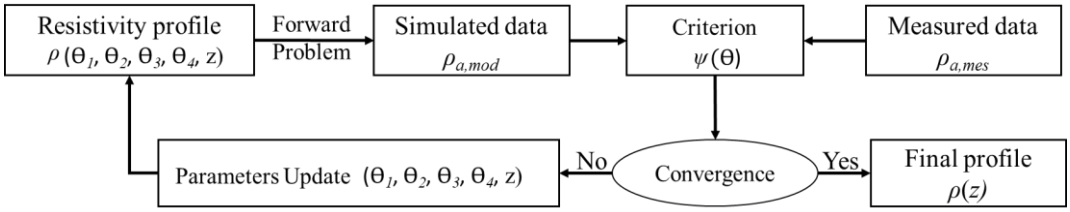

Figure 3: Inversion scheme of the apparent electrical resistivity used in CERIS method

2.2.3.Chloride profiles: step 3

The **Step 3** entails to convert the resistivity profiles obtained in **Step 2** to chloride profiles using the calibration curves obtained by a calibration campaign described in §3.4. The calibration campaign establishes the calibration laws which are corresponding to the real resistivity versus the free and total chloride concentration (Figure 2). To obtain these calibration laws, the electrical resistivity of many cores of the same concrete saturated with different sodium chloride concentrations was measured using the calibration resistivity cell [34]. At the end, the chloride content profiles obtained by NDE will be compared with those found by DE at the same exposure periods in section 4.

3. Materials and experimental protocol

The concrete mixes (C1 and C3) used in this work will be presented as well as the protocol followed to determine the DIs determined at 90 days and 6 years of curing age. Afterward, the slabs and the cores (nomenclature, dimensions, conditioning, etc.) used in the diffusion and calibration campaign are displayed.

3.1. Materials: Concrete mixes (C1 & C3)

In this work, the concrete slabs used were casted and demolded in 2013. The slabs were completely immersed in tap water after their casting until the start date of the diffusion campaign in September 2019. Two concrete mixes were used in this work: C1 and C3 (see Table 1). The two concretes are intended for short-term exposure period which requires an important contrasting gradient. Thus, the water/cement ratio was chosen to be greater than 0.6 (0.623 for C1 and 0.681 for C3) to accelerate the transport process to get significant measurements in a short period. The origin and quantity of aggregates are almost identical between the two materials. These concretes are quite similar in composition except for the nature of the cement. The main and the chemical composition of each cement used for the two concretes are displayed in

Table 2.

Table 1: Concrete mix design of concretes C1 and C3

Constituents (kg/m³ of concrete)	**Concrete C1**	**Concrete C3**
Aggregate (6/10)	320	320
Aggregate (11/22)	760	760
Sand (0/2)	560	430
Sand (0/4)	300	430
CEM I 52,5 N CE CP2 NF	305	-
CEM III/A 52.5 L PMES CP1 NF	-	260
Calcareous filler addition	-	50
Sika Prise SC2	0.7	-
Sikaplast Techno 80	-	1.9
Effective water	190	177
water/cement (w/c)	0.62	0.68
water/binder (w/b)	0.62	0.58

Table 2: Main and chemical composition of CEM I and CEM III

Main composition (% by weight)	**CEM I 52,5N CE CP2 NF**	**CEM III/A 52.5 L PMES CP1 NF**
Clinker	98.00	36.00
Slag	-	**62.00**
Filler	2.00	2.00
C_3S	63.49	69.10
C_2S	12.60	7.10
C_3A	8.09	11.80
C_4AF	9.80	6.20
Chemical composition (% by weight)		
CaO	64.53	50.50
SiO_2	20.12	29.2
Al_2O_3	5.03	8.20
Fe_2O_3	3.12	1.00
MgO	0.98	5.00
K_2O	0.98	0.29
Na_2O	0.16	0.28
SO_3	3.34	2.74
Cl^-	**0,01**	**0.32**

The binder of concrete C1 is an ordinary cement CEM I 52,5N CE CP2 NF while that of concrete C3 is composed of 84% of CEM III/A 52.5 L PMES CP1 NF and 16% of Calcareous filler addition. The cement CEM III/A, containing 62% of slag and 38% of clinker, is particularly used for structures in a maritime environment [46]. It can be seen that the concentration of chlorides in CEM III is 30 times higher than that of CEM I. This increase was caused by the using of alternative fuels in its manufacture [47]. These values of chloride content

could be used in order to find the initial chloride content in the concretes, which it could be compared to that obtained by DE.

3.2. Protocol to obtain the concrete's DIs, pore size distribution and pore solution properties

Two DIs were studied for both concrete: the porosity accessible to water Φ (%) and the apparent chloride migration coefficient $D_{a(mig)}$ (m²/s). Both durability indicator (DI) have been determined at short curing period (90 days) on three cylindrical cores (ϕ=75mm; h=70mm) for each indicator. The DIs were also determined at long curing period on three cylindrical cores (ϕ=50mm; h=50mm) extracted from slabs being submerged in water during 6 years of curing. The porosity accessible to water was measured by means of hydrostatic weighing [48] as well as the apparent diffusion coefficient $D_{a(mig)}$ was determined by migration test in non-steady state according to the NT BUILD 492 [49].

Moreover, the pore size distribution was also assessed with Mercury Intrusion Porosimetry (MIP), for both concrete at 6 years of curing, using an Autopore type IV 9500 V1.09. Two samples of each concrete were tested to study the repeatability of the results. The samples of approximately 3 cm^3 in volume (1×1.5×2 cm) were extracted from cylindrical cores with a micro-saw and then oven-dried at 60 °C until reaching a constant mass. This temperature was chosen to avoid hydrates deterioration [50]. Indeed, the pore size distribution was not determined at 90 days of curing. Therefore, the pore size distribution results found by Fabien et al. 2021 [51] at 90 days of curing, for concretes quite similar to C1 and C3, were used to study the evolution of the concrete's microstructure.

Besides, the pH and the electrical conductivity (σ_s) of the pore solution were determined for both concrete. For each concrete, one core (ϕ=50mm; h=50mm) was extracted from a saturated slab where it was then grounded in several steps with an average of 5 mm for each step, using a grinding instrument (German instrument®). The procedure recommended by RILEM association [52] were used to extract water-soluble ions by diluting grounded powder with distilled water. The determining of water-soluble ions could be realized with a more reliable test by extracting the pore solution from concrete using a hydraulic press [53]. The advantage of this method lies in its high reliability by avoiding errors uncertainties coming from concrete grinding and ions extraction. In this work, the measurements of the pH and the electrical conductivity were carried out on the water-soluble ions obtained for each 5 mm by using a pH-meter and a conductivity-meter. The pH-meter used consists of a combined electrode of two

electrodes including a calomel reference electrode and another glass electrode. An electric current is applied between the two electrodes in order to measure the electrical potential and then convert it to a pH value between 0 and 14.

3.3. Slabs conditioning chloride diffusion campaign

In this work, the chloride diffusion campaign was carried out on 2 slabs for both concrete 'C1 and C3'. The campaign was realized under saturated conditions to ensure pure chloride diffusion under a concentration gradient between the external and the interstitial solution. Accordingly, slabs were saturated under vacuum with tap water before being submitted to diffusion campaign. In addition, the first centimeter of each slab surface was cutted before the saturation process in order to remove any carbonated portion of the concrete due to the long curing time.

Table 3: Slabs conditioning

Nomenclature	Concrete	External solution		Dimensions (cm)
		[NaCl]	[NaOH]	
C1-35	C1	35 g/L	4 g/L	34 × 22 × 11
C3-35	C3			
C1-90	C1	90 g/L	4 g/L	
C3-90	C3			

The slabs had been also sealed laterally with epoxy resin to ensure unidirectional diffusion and to prevent the slab from drying. In addition, a small basin filled with tap water had been created by taping the border of the top face with aluminum foil (see Figure 4.a). The slabs were placed separately in closed boxes where the bottom face was immersed up to 1 cm, at initial test time t_0, in regularly renewed solutions with different sodium chloride concentration as depicted in Table 3. In order to avoid leaching of hydroxide ions from concrete, 4 g/l of NaOH were added in the external solution for all the slabs. At each test time, slabs were removed from boxes and the top and bottom face were wiped with two different sponges to remove the liquid water or solution. Then the apparent resistivity measurements were performed, using the protocol described in Figure 1 (see §2.1), for an exposure period of 1 day, 3 days, 1, 4, 10, 12, 14, 19, 21, 27 and 46 weeks for all the slabs so almost 11 months for the last exposure period.

In order to validate chloride profiles obtained by ERT, a DE campaign was carried out to find the 'real chloride profile' considered as reference profile. Three cores were extracted from each slab at 12, 19 and 46 weeks of exposure. These cores were grounded in several steps of an average of 5 mm for each step, perpendicular to the bottom face exposed to NaCl solution,

using a grinding instrument (German instrument®) as recommended by Vennesland et al. (2013) [54].

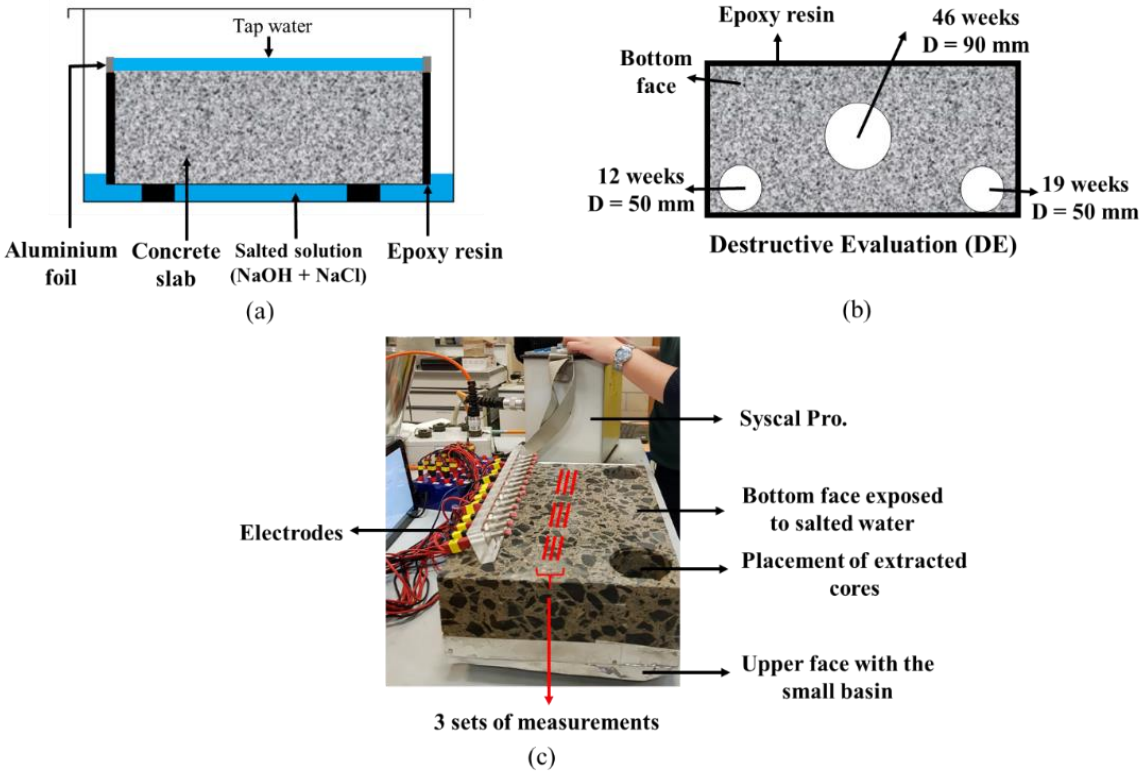

Figure 4: Diffusion campaign with DE and NDE: (a) Scheme of chloride diffusion installation presenting the cross-section area of slab, (b) top view displays the position of core extraction for DE, (c) ERT measurements at 46 weeks of diffusion before extracting cores for DE

The procedure recommended by RILEM association [52] was used to extract water-soluble ions including **free** chlorides ions. As regards the problem of distinguishing experimentally between free and bound chlorides, the contact time between powdered concrete and water to extract free chlorides is fixed at 3 minutes to avoid any calcium chloro-aluminate (Friedel's salt) dissolution [55]. Moreover, the **total** chloride ions were extracted from concrete powder following the recommendations of AFREM association (1992) [55]. Thus, concrete powder putted into suspension in nitric acid and agitated until boiling (T=80°C) during 30 minutes to extract bounded chlorides. Finally, the free and the total chloride concentration was determined by potentiometric titration.

3.4. Cores preparation for calibration campaign

Six cores for both concrete were extracted from slabs (ϕ=75 mm) and sawn to have a similar thickness (h=70 mm) as that of the electrical resistivity cell (see Figure 5.a).

For each concrete, the 6 cores were oven-dried at 60 °C until mass stabilization and were then saturated under vacuum with solutions having 3 sodium chloride concentrations '[NaCl] = 0, 35 and 90 g/L' (2 cores by concentration). Moreover 4 g/L of NaOH was added in these solutions to avoid leaching.

After two days of cores saturation, the electrical resistivity measurements were performed using the resistivity cell [34]. The principle is as follows: Five ring electrodes were positioned inside a cylindrical PVC framework to create the cell (see Figure 5.a). In order to provide greater contact with the concrete during the test, the electrodes are formed of conductive metallic sponges that have been thoroughly humidified before use. Two metallic plate electrodes are positioned on the top and bottom ends of the core, respectively, as depicted in Figure 5.b and an electrical current of intensity I is injected through them. Then, in order to evaluate the homogeneity of the core, potential differences ΔV_i are measured between the various ring pairings. Next, using following equation ($\rho_{ai} = G_i . \Delta V_i / I$), the apparent resistivity ρ_{ai} for each pair of rings is determined, where G_i is the geometric factor calculated using the COMSOL Multiphysics finite element software and account for both the electrode spacing and the core geometry. Six measures are made as a result: two measurements are taken between the two extreme rings and four measurements are taken between each two consecutive rings. The resistivity of the concrete cylinders could be also determined using the wenner probes as depicted in the study of Morris et al. [56]. The findings of Du Plooy et al.[34] showed that the resistivity values measured with the resistivity cell used in this work and the wenner probes have a very good correclation (R^2=0.9931), for the same concrete cores.

Considering that the cores are homogeneous (same chloride content along depth), the measured electrical resistivity is considered as 'the real resistivity'. Two sets of measurements were realized by measuring the resistivities in the two directions of the core. The total number of measurements is also 12 per core. Thus, the average of these 12 measurements and the standard-deviation were calculated to get the ordinate of calibration curves.

In order to determine the chloride concentration for each core which will represent the abscissa of the calibration curve, a DE campaign was carried out at the end of the resistivity measurements. The steps are described in Figure 5.b. The cores were sawn into three parts, then each part was grounded with a vibrating disc mill RS200® to obtain a powder with 20 µm of fineness. The free and the total chloride concentration is then determined for each part by using

the same procedure mentioned in §3.3. The average of the three chloride concentrations (free and total) was used to determine the abscissa of calibration curves.

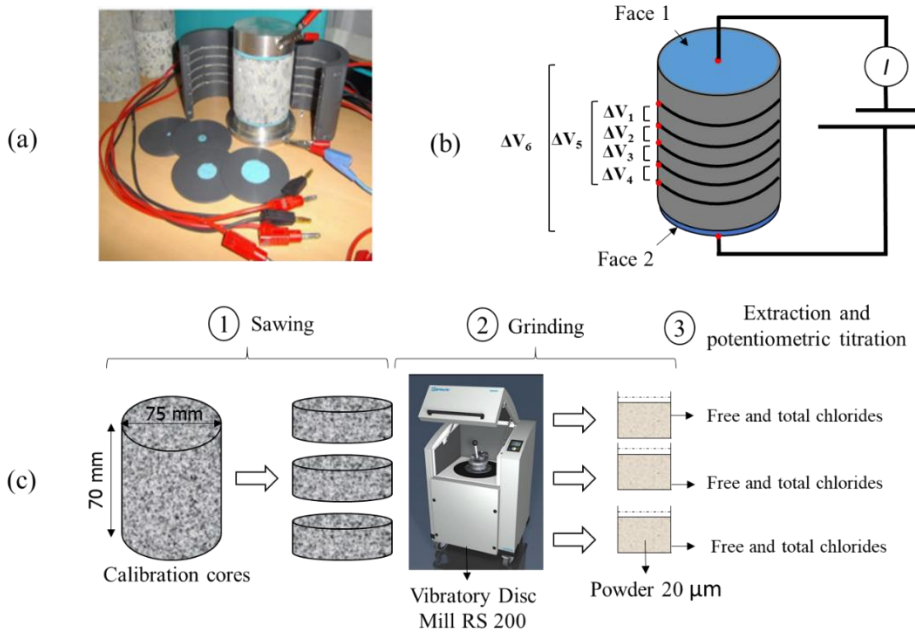

Figure 5: Calibration campaign (a) Resistivity cell, (b) position of potential difference measurements, (c) Protocol to determine the chloride content by destructive test in the calibration cores

4. Results and discussion

In this section, the DIs determined for both concrete at a short (90 days) and long (6 years) curing period are displayed firstly. Secondly, the calibrations curves, which relate the real electrical resistivity with the free and the total chloride concentrations are presented. Moreover, the effect of the BFS incorporation on the electrical resistivity were studied by comparing the resistivity of both concrete. Finally, the free and total chloride concentration profiles obtained by the DE methodology are analyzed before comparing with the NDE chloride profiles at three different exposure periods (12, 19 and 46 weeks).

4.1. Effect of long curing period on DIs, MIP measurements and pore solution properties

4.1.1. Durability indicators (DIs)

The porosity accessible to water of both concrete at 90 days and 6 years of curing are displayed in Table 4. The values displayed are the average (μ) of the three samples as well as the standard deviation (σ). The differences between the porosities obtained at 90 days and 6 years are almost negligible, with a porosity for concrete C1 quite similar to that of C3. We can then conclude

that the porosity for both concrete had not changed at 6 years of curing. These results are similar to those of Ben Fraj et al. (2012) [12] who have shown a negligible effect of slag on the porosity at a short curing period (90 days). Moreover, Fabien et al. [51] found a negligible increase in the porosity of BFS concrete compared to that obtained for ordinary concrete. The researchers also explained the small increase of the BFS concrete porosity to the high sensitivity of slag to the high oven-dry temperature (105 °C). In order to deepen these results, it is necessary to study the evolution of the microstructure results presented in §4.1.2.

Table 4: Durability indicators and properties of pore solution for both concrete (C1&C3)

			C1		C3	
			μ	σ	μ	σ
Durability indicators	Open water porosity (%)	**90 days**	16.20	1.19	15.97	0.33
		6 years	15.88	1.33	15.9	0.14
	$D_{a(mig)}$ ($\times 10^{-12}$ m²/s)	**90 days**	28.30	3.74	5.83	0.61
		6 years	31.10	2.97	3.73	0.28
Properties of pore solution	pH (-)	**6 years**	11.47	0.41	9.57	1.22
	σ_s (µS/m)	**6 years**	1558.7	415.98	225.87	54.8

As the porosity value, the $D_{a(mig)}$ values displayed are the average (μ) of the three samples as well as the standard deviation (σ). According to the five potential classes suggested by Nilsson et al. (1998) [57], the results obtained at both curing period show a weak resistance to chloride ingress for concrete C1 ($D_{a(mig)}$>20.10^{-12} m²/s) whereas a very strong resistance for C3 ($D_{a(mig)}$<5.10^{-12} m²/s) (c.f. Table 4). These results present the same tendency as that presented in the studies of Baroghel-Bouny et al. (2011), Duan et al. (2013) and Teng et al. (2013), which is explained by the small micro-porosity of concrete C3 leads to a higher tortuosity and consequently to a lower diffusion coefficient of chlorides [58].

We can also notice a decrease in the diffusivity of concrete C3 at 6 years of curing compared to that found at 90 days (5.8 to 3.73 $\times 10^{-12}$ m²/s). Whereas the diffusivity for C1 increases by 9% compared to that obtained at 90 days of cure and a standard deviation equal to 2.97 ($\times 10^{-12}$ m²/s). Indeed, the slag leads to an increase in chloride binding thanks to the chemical reaction between the chlorides and the aluminates more numerous in slag [12,59,60], which helps to slow the chloride diffusivity into concrete. However, chloride binding could not affect the value of the $D_{a(mig)}$ since the period of the migration test is very short (6-8 hours for C1 and 24—27 hours for C3): so binding is supposed to not occur [6]. According to Spiesz et al. [61], the binding is not complete during the rapid migration test, because it is not an instantaneous process. Thus, for higher concrete resistivity where samples take place for longer exposure,

more chloride ions are bound, and then less free chloride ions penetrate further and, consequently, a smaller Da tends to be obtained. We can therefore conclude that these results should be more related to the evolution of the microstructure of concrete during cure period.

4.1.2. MIP measurements

In order to explain the results obtained for the chloride diffusion coefficient, it was necessary to study the microstructure of both concrete and their evolution with curing time by MIP. The critical diameter d_c was determined from the inflection point of the curve representing the cumulative volume of mercury having penetrated the sample according to the injection pressure, i.e. the peak of the curves presented in Figure 6. The results obtained for concrete C1 are displayed in blue color and those obtained for concrete C3 in green color. The same color format will be used for all the other results.

The results obtained at six years of curing show a good repeatability between the two samples of the same concrete with a pore diameter range between 6 and 200 nm for concrete C3 (C3-1 and C3-2) whereas a greater range for concrete C1 (C1-1 and C1-2) between 60 and 600 nm. The critical diameters d_c for samples C1-1 and C1-2 are equal to 183 and 226 nm, respectively. However, the critical diameter for concrete C3 is much smaller and several peaks could be observed in the nanopores at 6, 11, 40 and 100 nm for the two samples.

These results showing a smaller critical diameter for concrete C3 have the same tendency as the experimental findings in the literature [14,30,51,53,62–64]. The decrease in the pore size diameter 'd_c' was explained by the refinement of the pores thanks to the formation of new C-S-H gels during the pozzolanic reaction and the small average particle size of BFS compared to those of PC. It should be noticed that in the literature, all the MIP tests were carried out at short curing ages (28 and 90 days). Thus, the critical diameter for the tested concrete with BFS was larger than that obtained in this work (6 years of curing).

Fabien et al. (2021) [51] studied the pore distribution for two concretes quite similar to those of C1 and C3 but at 90 days of curing. We can notice an important reduction in the critical diameter obtained after 6 years of curing for concrete C3 compared to those obtained by Fabien et al. (2021) at 90 days with a d_c passes from nano- to micro-meter (see Figure 6). This decrease is due to the complete hydration of all anhydrous after 6 years of curing and the completion of the hydraulic reaction for concrete C3. On the other hand, a small increase in the critical pore size diameter d_c for concrete C1 is noticed after 6 years of curing. These interesting results explain the decrease of $D_{a(mig)}$ for concrete C3 after 6 years of curing. We can conclude that

the very strong chloride diffusivity of concrete C3 after 6 years of curing is connected to two important effects: the complete hydration of slag, which leads to a refinement of the microstructure.

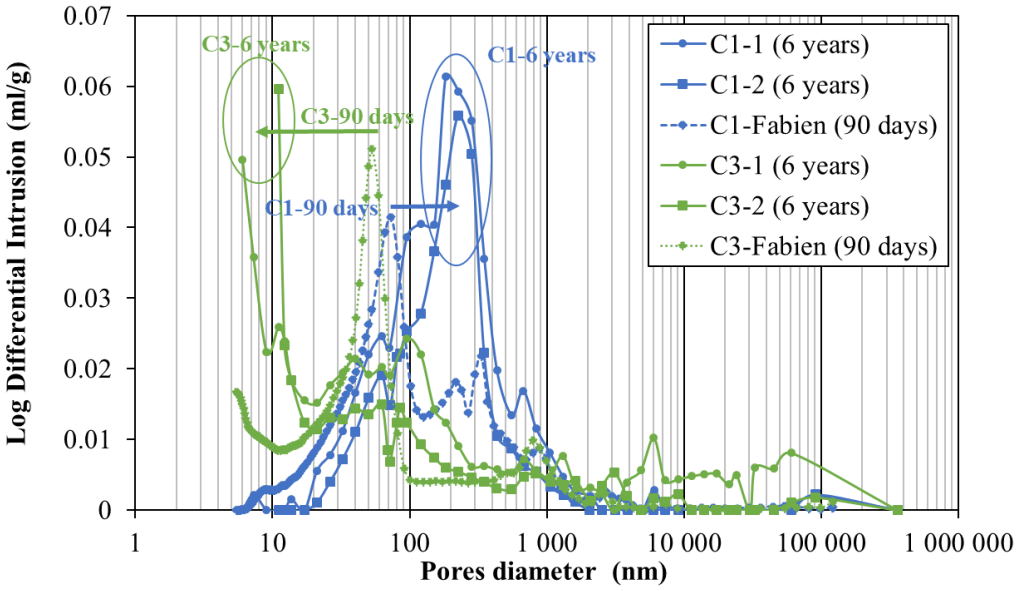

Figure 6: Differential pore size distribution values obtained at 6 years for concrete C1 and C3 compared with those obtained by Fabien [51] at 90 days for similar concretes

4.1.3.pH and electrical conductivity of the interstitial solution

The average value of the electrical conductivity and the pH of the interstitial solution are presented in Table 4 as well as the standard deviation. The results show an electrical conductivity seven times lower for concrete C3 than that of concrete C1. The findings of [65] et al. (2012) agree with our results where they found an increasing in the electrical conductivity of the pore solution when the Portland cement is partially substituted by BFS. Medeiros-Junior and Lima (2016) [33] explained the increase of the electrical resistivity of BFS concrete by the decrease in the quantity of hydroxide ions (OH^-) over time in the pore solution. The reduction in the hydroxide ions content caused by the consumption of portlandite during the pozzolanic reaction leads to an important decrease in the electrical conductivity of the pore solution and consequently to an increase in the electrical resistivity of the concrete.

Furthermore, the results of Cherif et al. (2020) [64] show that the hydroxide concentration is 1.7 times lower in the pore solution of concrete with BFS (75% of blast furnace slag on the mass of binder) than a typical concrete without BFS. In this work, the decrease in the quantity of hydroxide ions was leading to lower the pH of the pore solution of concrete C3, with an average value equal to 9.57 for concrete C3 and 11.47 for concrete C1. The pH values obtained

for concrete C1 and C3 are lower than those obtained in the literature for similar concrete [53,66]. It seems that the method used to extract water soluble-ions can significantly influence the value of pH and electrical conductivity. The leaching and pressing method applied, respectively, in the work of Liu [66] and Cherif et al. [64] seem to be more reliable than that used in this work because of the uncertainties that may be brought during the several steps of the current method (grinding, soluble-ions extraction, dilution). However, the approach adopted in this work provides the advantage of determining profiles of pH, electrical conductivity and ion concentration, which help to understand the tendency variation due to chloride diffusion. Thus, the effect of the water soluble-ions extraction method should be studied in a future work.

4.2. Calibration results

Before analyzing the calibration curves at 6 years of curing presented in Figure 7, it's worth mentioning herein that the electrical resistivity of both concrete was determined at 90 days of curing but only for the cores saturated with tap water without chlorides [23]. The results show an electrical resistivity for concrete C3 (356 Ω.m) 7 times bigger than that of C1 (52.7 Ω.m). The MIP results obtained at 90 days justify the higher electrical resistivity for concrete C3: the critical pore diameter d_c of C3 is 1.5 times lower than that of C1, which means a higher tortuosity for C3 leading to reduce the electrical current flow (see Figure 6 and Table 4).

It's important to note that the resistivity values obtained along the cores at 6 years (at the different positions) are nearly identical (low values of standard deviation) which ensures that the concrete's resistivity is uniform.

At 6 years of curing, we can notice that the electrical resistivity of C1 remained constant (52.16 Ω.m) by comparing with the value obtained at 90 days whereas the electrical resistivity of C3 was multiplied by 1.5 to reach 534 Ω.m at 6 years (see Figure 7). These resistivity values are in the same range (300-1000 Ω.m) of that obtained, in Polder report [67], for BFS concrete (>65% slag) of mature structure (>10years) in submerged zone. Additionally, the findings in the Y. Liu dissertation [66] showed resistivity values (400 Ω.m) that were comparable to those reported for C3 after 6 years, but for slag concrete at 1 year of curing that had undergone an accelerated curing at short age. The pozzolanic reaction of BFS which was achieving between 90 days and 6 years of curing was leading to produce a new hydrates of C-S-H gels. Thus, the pore size diameter dc of C3 determined at 6 years is 20 times lower than that obtained at 90 days. Consequently, the electrical resistivity of concrete C3 increased. Furthermore, the higher resistivity of C3 determined at 6 years, is also linked to the the pore solution electrical

conductivity which is 7 times lower for concrete C3 compared to that of C1, (see Table 4). This low value of pore solution conductivity for C3 is linked to the consuming of the hydroxide ions (OH^-) during the pozzolanic reaction, which could be explained by the low value of pH (9.57 ± 1.22) measured at 6 years. Therefore, it could be concluded that the decrease in the pH of the poral solution induced by the decrease in the concentration of hydroxide ions leads to an increase in the electrical resistivity of this solution and consequently to an increase in the concrete resistivity. Therefore, we will notice that the concrete resistivity decreases when the chloride content increases in the pore solution. Unfortunately, the pore solution conductivity and its pH were not determined at 90 days, which make impossible to study the relationship evolution of the pore solution characteristics and the concrete resistivity over time. Nevertheless, this relationship is very clear by showing the effect of BFS on the pore solution characteristics and the concrete resistivity and by comparing these characteristics for both concrete.

In addition, we can notice that the chloride concentration found by DE of concrete C1 is higher than that obtained for concrete C3 for the cores saturated with the same sodium chloride concentration (see Figure 7). These results can also reveal the low diffusivity of concrete C3 even before determining the chloride profiles obtained during the diffusion campaign submitted on the slabs. It is worth mentioning herein that the initial chloride concentration obtained by DE for the cores saturated with free chloride tap water ([NaCl]=0g/L) is noticeable for both concrete. The initial free chloride concentration exhibits 0.00025 and 0.00045 g/g of concrete for C1 and C3, respectively. As well, the initial total chloride concentration exhibits 0.0003 and 0.00057g/g of concrete for C1 and C3, respectively. It can be seen that the free or total initial chlorides concentration in concrete C3 is two times bigger than that obtained in C1. Indeed, the chloride ions can be imported into concrete from their own constituents such as the binder, the sand or the tap water. Due to the fact that both concrete are quite similar in composition excepting the nature of the cement, the increase in the initial chloride concentration can be explained by the higher amount of chlorides in CEM III (cf.

Table 2).

As expected, the electrical resistivity decreases progressively for both concrete with the increase of the chloride concentration. With 35 and 90 g/L of NaCl, respectively, the concrete resistivity of C1 loses 60 and 70% of its initial value (without chloride). Similar to concrete C1, concrete C3 loses 71% and 85% of its initial value when exposed to 35 and 90 g/L of NaCl, respectively. Thus, the resistivity measurement displays a fast decrease for low chloride concentration ([NaCl]=35g/L) while a slow decrease for high chloride concentration

([NaCl]=90g/L) for both concrete, similarly to the results obtained for Portland concrete [20,23,68,69]. The steepness of the slope of the fitted calibration curve demonstrates this non-linearity in the change rate of the resistivity-chloride content. The calibration curves were obtained by fitting the experimental resistivity values using a power function [70] with a regression coefficient superior to 0.9 for the measurements carried out at 6 years.

These calibration curves obtained will be used to determine the free and total chloride profiles of the slabs during the diffusion campaign. In this paper the free and the total chloride profiles will be determined in order to study the effect of slag on concrete chloride binding capacity. For both concrete, the calibration curves for the total chloride are upward shifted compared to that obtained for free chloride. In addition, fitting the calibration measurements with a power law gives a steep calibration curve at low concentrations and horizontal curve at high concentrations which leads to find a higher chloride concentration for low resistivities especially when the total chlorides calibration curves are used.

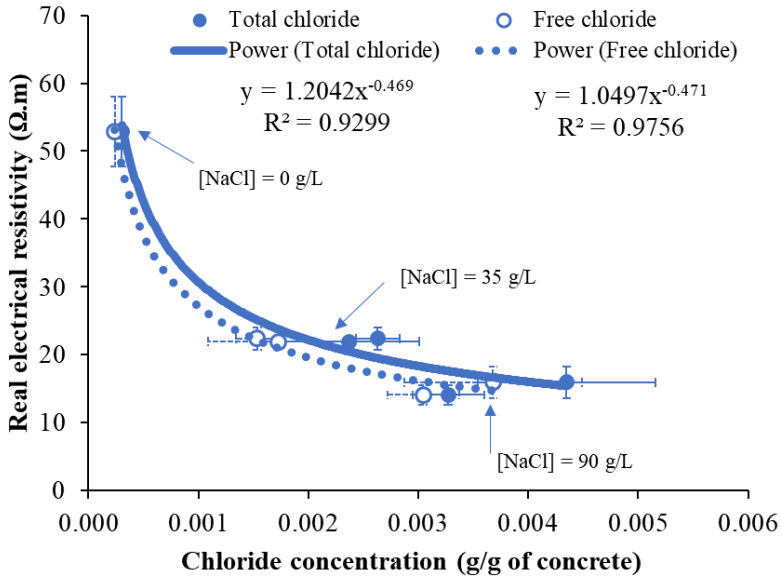

(a)

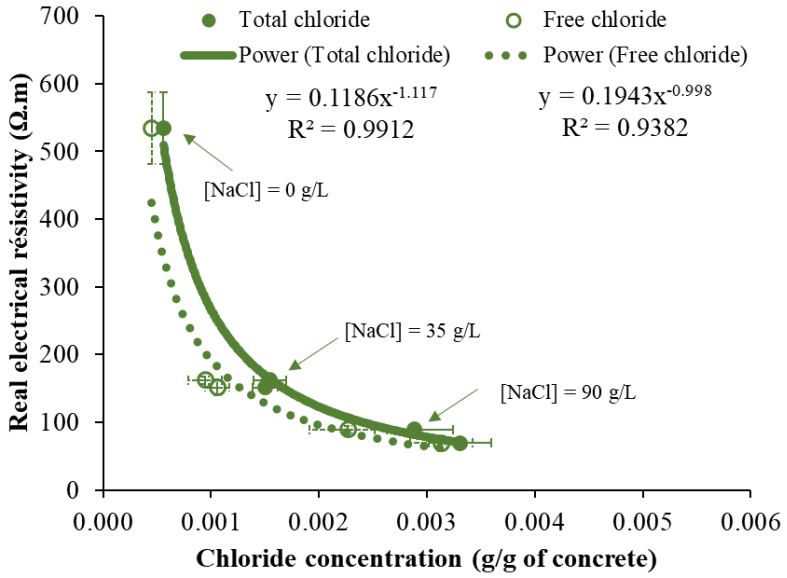

(b)

Figure 7: Calibration curves of electrical resistivity as a function of free and total chloride concentration after 6 years of curing: (a) Concrete C1, (b) Concrete C3

4.3. The apparent resistivity results and the real resistivity profiles (step 1 & 2)

The apparent resistivity values were obtained for the four slabs (C1-35, C1-90, C3-35 and C1-90) during the diffusion campaign. For example, the apparent resistivities for slab C3-35 versus diffusion time are presented in Figure 8. As the slabs were saturated under vacuum with tap water to obtain a homogeneous slab (same chloride and water content along depth), thus the apparent electrical resistivities measured by the ERT device at initial test time t_0 for the 4 electrodes spacing/Levels were expected to be equal. However, the apparent electrical resistivity at Level 1 (nearest Level to the external ambient) is slightly higher than those of other deeper Levels (2, 3 and 4) which indicates an initial property gradient in the concrete. The origin of this gradient could be due to an ionic difference in the material due to leaching. Indeed, the concretes were stored in tap water during 6 years and leaching may have occurred, even if the first centimeter of each slab surface was sawn and removed before the saturation process.

For both slab of concrete C1 and C3, the apparent resistivity values for the 4 Levels decreased instantly, as expected, with the beginning of the diffusion campaign due to the penetration of chlorides ions. As expected, within a few days of chloride diffusion, the lowest apparent resistivity is located at the nearest Level to the external surface (Level 1) whereas the highest resistivity is located at the farthest Level to the external surface (Level 4). The higher apparent resistivity in-depth reveals a lower concentration and a higher chlorides concentration on the surface which agrees with the direction of chlorides ions propagation.

For both slab of concrete C3, the electrical resistivity for level 1 remained constant after one month of diffusion until the end of the campaign. However, between the first and the sixth month of diffusion, an increase in the apparent resistivity is noticed for the 3 Levels (2, 3 and 4) which can be explained by the late binding of chloride with the cement matrix producing the formation of Friedel's salt (see Figure 8). The chloride binding in concrete C3 due to the chemical reaction of chlorides with aluminates leads to the formation of Friedel's salt which influences the microstructure of the concrete. Shi et al. (2017) [71] showed that the porosity of BFS concrete decreases linearly with the increase of Friedel's salt content. The decrease of the microstructure of BFS concrete during diffusion campaign could be one of the reasons leading to the increase of the electrical resistivity as explained before in section 4.2.

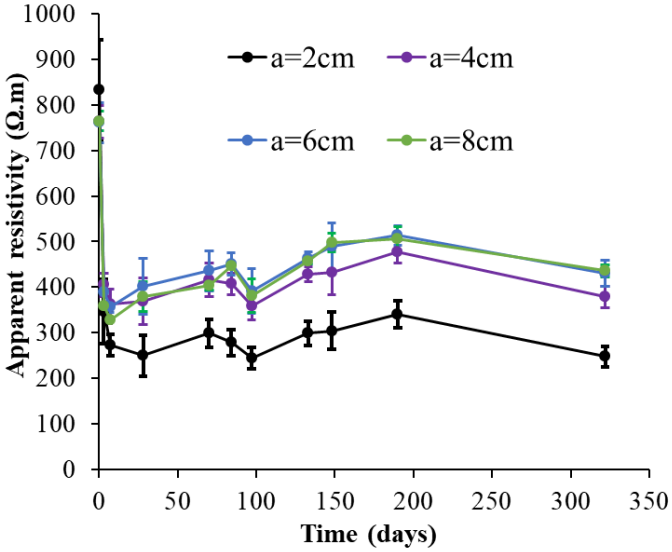

Figure 8: Apparent resistivity for slab C3-35

In addition, we can notice a suddenly dropped in the apparent resistivity at 100 day at all levels. Many factors could affect the surface resistivity measurement such as the ambient temperature [67,72,66,73,74]. The temperature of the concrete influences the concentration and mobility of the ions and the ion-solid and the ion–ion interactions. In the laboratory where the experimental campaign was carried out, it appears that the air conditioners malfunctioned during this time, causing the temperature to rise and, as a result, the resistivity to decrease. Another factor could affect the concrete resistivity is the measurement time compared to the renewal time of the saline water. It seems that, in contrast to other measurements, which were typically made two weeks following the renewal of saline water, the resistivity measurements at 100 days of diffusion were made just one day after the water renewal. As a result, the chloride binding was

not stable, which caused more free chlorides to be present in the pore solution and a subsequent decrease in concrete resistivity.

The apparent resistivity of the four slabs was inverted with the two different methods (Res1D and CERIS) to determine the real resistivity profiles versus depth. The real resistivity profiles for the slab C3-35 obtained by Res1d and CERIS inversion are presented in Figure 9.a. and Figure 9.b., respectively. As already mentioned, the resistivity profiles inverted by Res1D are finally represented in 4 layers of different thicknesses while those inverted by CERIS are represented in the form of curves thanks to the continuous parameterization. The profiles shape obtained by inversion (especially CERIS) show a logical evolution where we can clearly observe a lower resistivity at surface (5-15 mm) than that at depth over time indicating a bigger amount of chloride at surface. The profiles show a decrease in the resistivity until one month of diffusion, then a slight increasing of the resistivity related to the increase of the apparent values explained by chloride fixation and diffusion stability. Indeed, the addition of sodium hydroxide (4g/L) to the saline solution eliminates the possibility that the rise in resistivity is the result of concrete leaching during the test. After one month, the profiles are almost stable on the surface and in depth taking into account the cumulated uncertainties coming from measurement, sensitivity devices at depth beyond 40 mm and inversion. The resistivity profiles obtained for the three other slabs have almost the same behavior during the diffusion campaign but they will not be presented in this paper. These profiles will be converted in the next section to chlorides profiles by using the calibration curves displayed in Figure 7.

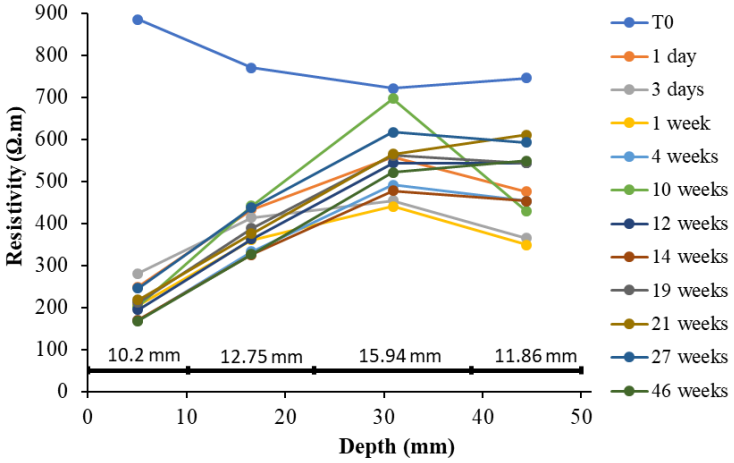

(a)

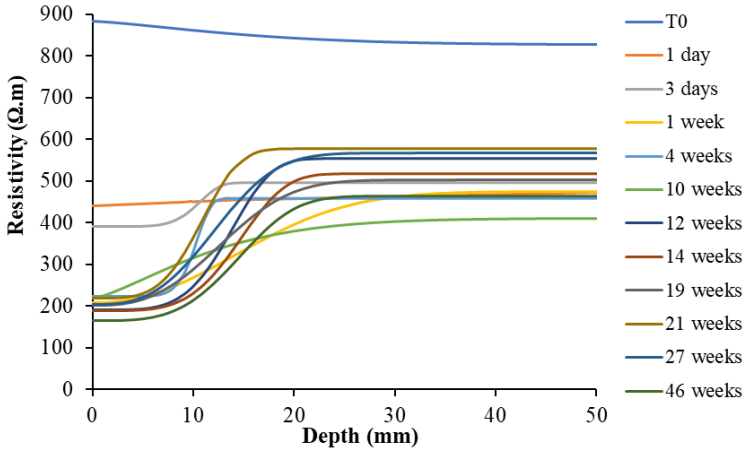

(b)

Figure 9: Real resistivity profile for slab C3-35 obtained: (a) inversion with Res1D, (b) inversion with CERIS

4.4. Free and total chloride profiles

In this sub-section, the evolution of free and total chloride profile obtained by DE were analyzed in order to study the effect of slag on these profiles. Then, the NDE chloride profiles were compared to those obtained by DE for the four slabs at three different exposure periods and the influence of using CERIS method was studied.

4.4.1. Evolution of free and total chloride content profiles (DE) with time

The free and total chloride content profiles obtained by DE at 46 weeks of diffusion for the four slabs are displayed in Figure 10. By comparing the results found for both concrete for any external NaCl concentration, we can notice that the profiles of concrete C3 have a steep shape; the chlorides are more concentrated near to the external surface exposed to the salt solution (from 0 to 15 mm) than in the deep of the slab (15 to 50 mm). These results can be explained by the low diffusivity of concrete C3 which is related also to the small pore structure of this concrete. Moreover, the high binding capacity of concrete C3 may be due to slow down the chloride diffusion, which leads to gather a big amount of chlorides close to the external surface. However, the high diffusivity of concrete C1 ($D_{a(mig)}$=31.1×10^{-12} m²/s) was the reason to obtain a merely constant profiles along depth where chlorides are evenly spread along the first 5 cm of the slab which reveals the fast chloride diffusion in concrete C1.

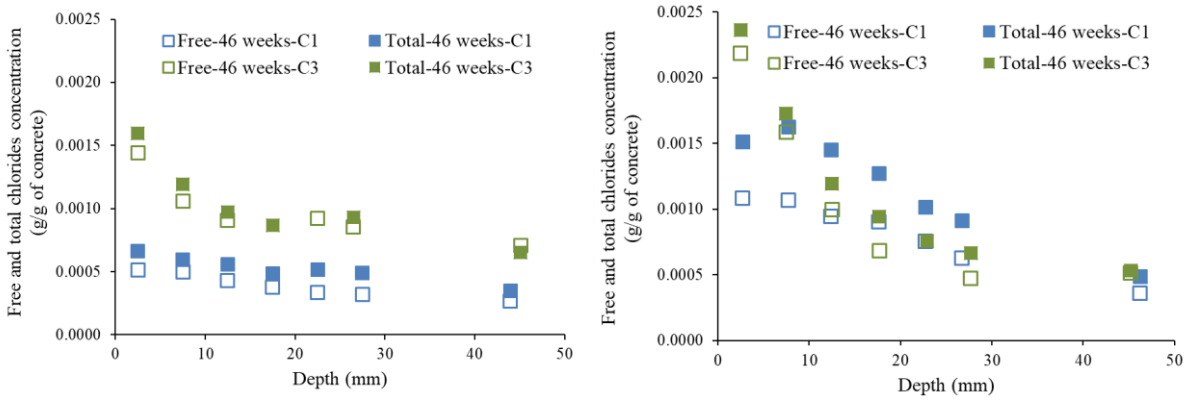

(a) [NaCl]=35 g/l (b) [NaCl]=90 g/l

Figure 10: Free and total chlorides content profiles at 46 weeks of diffusion

It can be noted that for the two slabs exposed to a low concentration of NaCl equal to 35 g/L, the chloride profiles (free or total) for concrete C3 are always higher than those of concrete C1 even at 46 weeks of diffusion. As mentioned earlier in section 4.2, the initial chlorides content in concrete C3 is 2.7 times higher than that in C1, thus the difference between the profiles for the two concretes even exists before the beginning of the diffusion campaign. This difference remained constant between the two concretes even at 46 weeks of diffusion. However, for a higher exposure concentration of NaCl equal to 90 g/L, it was observed that the chloride content at the surface (0 to 10 mm) for concrete C1 are lower than that for C3. The high concentration of chlorides in the external solution increases the contrast in chloride concentration gradient, which induces to increase the chloride flux. However, the chloride content for concrete C3 is lower than that of C1 in depth which represents the positive effect of BFS on the chloride diffusivity.

Furthermore, another factor could affect the chlorides profile as skin effect called also convection zone [75]. As this paper study the diffusion of chloride in totally submerged zone (saturated conditions), we can consider that the skin effect is not influential because none environmental conditions (rainfalls flushing, wetting-drying cycles, oxygen, carbonation, exposure time) are existing. However, in-situ test results have demonstrated that concrete exposed to the submerged zone, for more than 10 years, may also have a significant skin effect [76–79]. Researchers explained this effect by the dynamic equilibrium of the surface chloride concentration in the concrete with the ambient medium concentration and subsequently tends to stabilize because the transport process is driven by pure diffusion of chloride ions under a concentration gradient. As a result, the chloride profile obtained at several year of exposure are different that those determined at short period such 44 weeks. As case study, the skin effect

could be detected within the surface resistivity measurements by reducing the spacing between the electrodes to reach an investigation depth inside the convection zone.

4.4.2. Comparison between DE and NDE profiles

The free and the total chloride profiles obtained by NDE and DE, at three different diffusion periods 12, 19 and 46 weeks, for the slabs C1-35 and C3-35 exposed to [NaCl]=35 g/L are presented in Figure 11. As same as, Figure 12 gives the corresponding profiles obtained for the two slabs C1-90 and C3-90 exposed to [NaCl]=90 g/L. Each figure presents three chloride concentration profiles: (1) a profile obtained by NDE with CERIS inversion presented with a smooth solid line, (2) a second profile obtained by NDE with Res1D displayed with straight and marked solid line, (3) and a third profile obtained by DE presented with a straight and marked dash line. As regarding the uncertainty of DE profiles, Bonnet et al. (2020) [80] found that the coefficient of variation for total chloride content is equal to 6.8 %. Since the protocol used for obtaining the total chloride in the study of Bonnet et al. (2020) [80] is similar to that used in this work for the free chloride, the same coefficient of variation was used to determine the vertical error bars displayed in the Figure 11 and 12.

The steepness of the slope of chloride profiles obtained by ERT is higher for C3 than that of C1, similar to profile shape obtained by DE, which explains the low diffusivity of concrete C3 as mentioned before. These results are certainly related to durability indicators and porous solution characteristics. A low pH and electrical conductivity value indicates that the concentration of various ions (particularly hydroxydes) in the porous solution is inadequate, which slows the diffusion of chlorides, as well as steeper profiles. Similarly, the refinement of the microstructure to decrease the chloride diffusion coefficient, resulting in a buildup of chlorides on the surface.

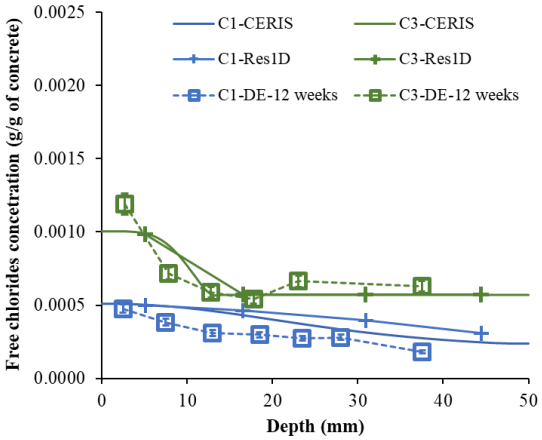

(a) Free-12 weeks

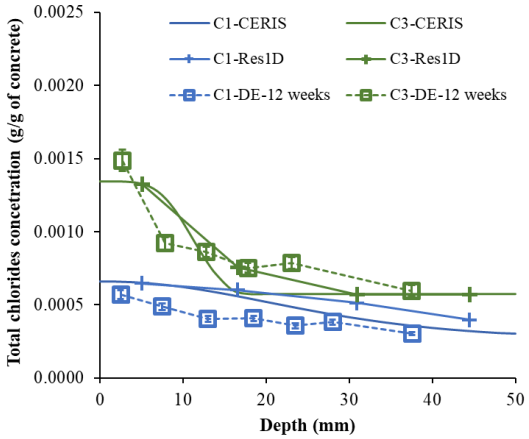

(b) Total-12 weeks

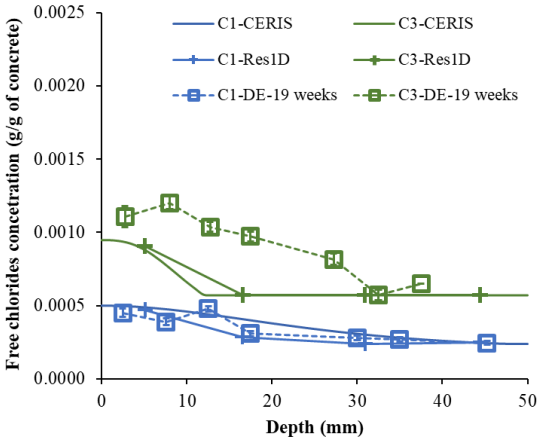

(c) Free-19 weeks

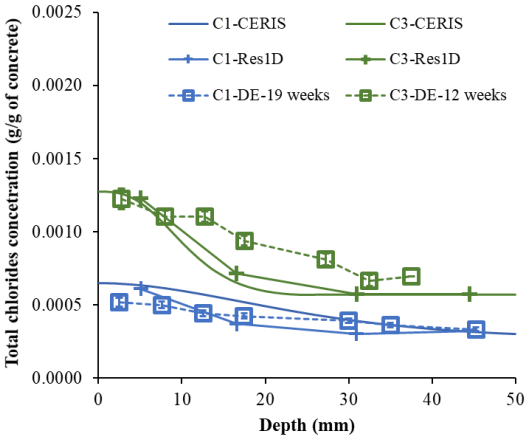

(d) Total-19 weeks

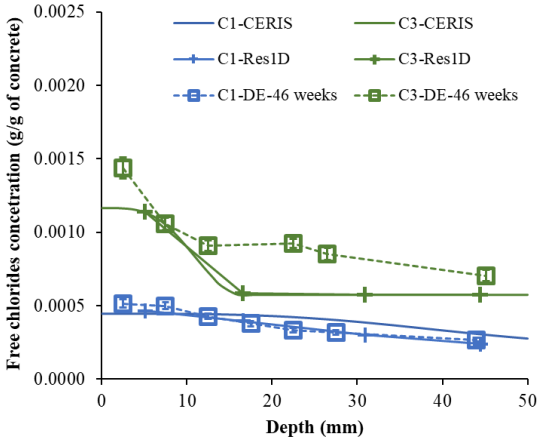

(e) Free-46 weeks

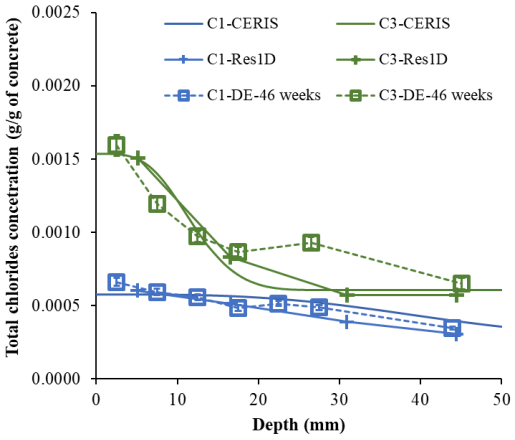

(f) Total-46 weeks

Figure 11: Free and total chloride concentration profile obtained by DE and NDE for slab C1-35 and C3-35 exposed to a [NaCl]=35g/L: (a) Free -12 weeks, (b) Total -12 weeks, (c) Free-19 weeks, (d) Total-19 weeks, (e) Free-46 weeks, (b) Total -46 weeks

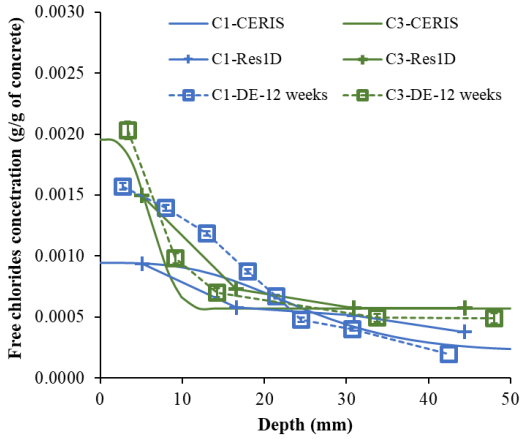

(a) 12 weeks – free chlorides

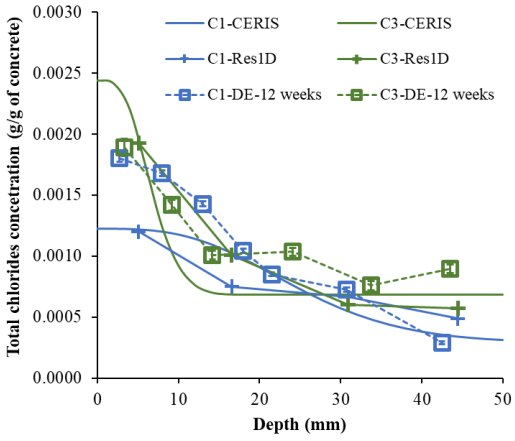

(b) 12 weeks – total chlorides

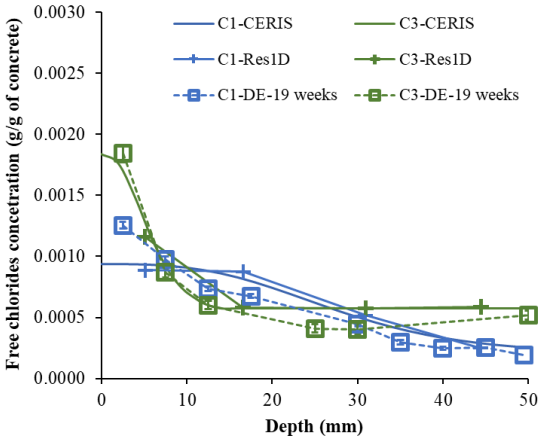

(c) 19 weeks – free chlorides

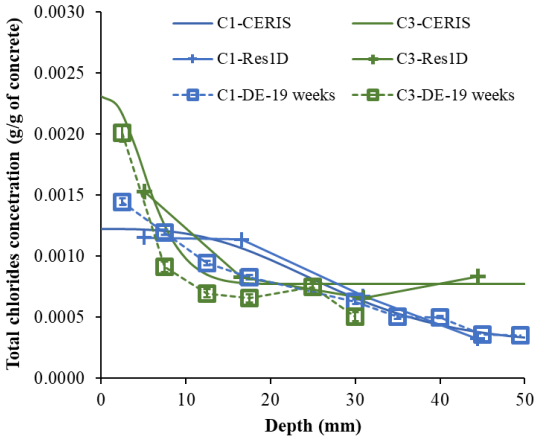

(d) 19 weeks – total chlorides

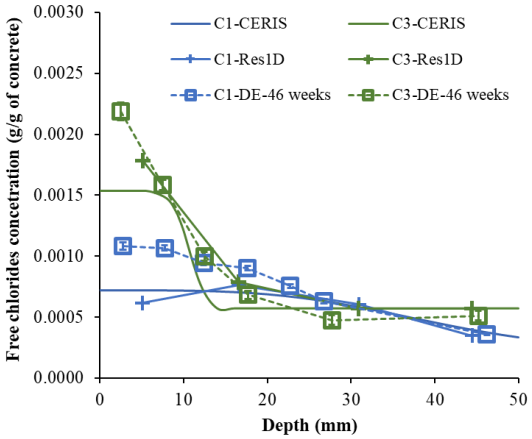

(e) 46 weeks – free chlorides

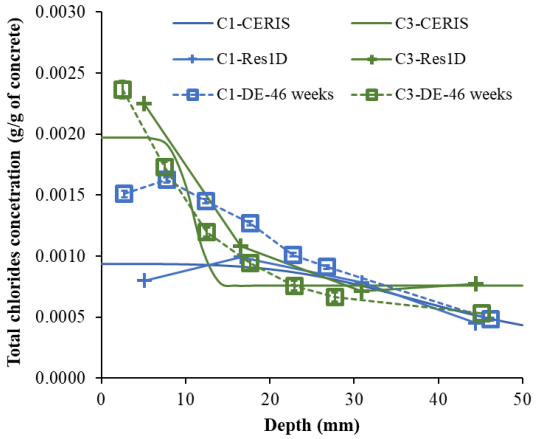

(f) 46 weeks – total chlorides

Figure 12: Free and total chloride concentration profile obtained by DE and NDE for slab C1-90 and C3-90 exposed to a [NaCl]=90g/L: (a) Free -12 weeks, (b) Total -12 weeks, (c) Free-19 weeks, (d) Total-19 weeks, (e) Free-46 weeks, (b) Total -46 weeks

Regarding the comparison between the NDE chloride profiles obtained by two inversion method (Res1D-CERIS), the results show a very good similarity between the two profiles at a given time with very small deviation. This small deviation due to the discontinuity of the Res1D profiles is more visible when passing from one layer to another. Moreover, the ND chloride profiles (CERIS or Res1D) show a good compatibility with those obtained by DE, especially for the slabs submitted to high chloride concentration (NaCl=90 g/L) where chloride gradient is more contrasted with an ERT device more sensible. In order to evaluate and quantify the difference between the DE profiles considered as 'reference profiles' and the NDE profiles, the RMSE 'Root-Mean-Square Error' was calculated using equation (3):

$$RMSE = \sqrt{\frac{\sum_{xi}^{n}\left[Cl^{-}_{ED,xi} - Cl^{-}_{END,xi}\right]^{2}}{n}} \quad (3)$$

with $Cl^-_{ED,xi}$ the free or the total chlorides concentration (g/g of the concrete) determined by the DE at a depth x_i (mm) and $Cl^-_{END,xi}$ the free or the total chlorides concentration (g/g of the concrete) obtained at the same depth by NDE. The RMSE values for the free and total chloride profiles are shown in Figure 13 and Figure 14, respectively.

Indeed, the small differences between the DE and NDE profiles can be attributed to several sources of uncertainty which could affect the reliability of the NDE and DE results. Concerning the NDE profiles, the process of obtaining the distribution of electrical resistivity from the apparent measurement can lead to error propagation. Many sources of error could affect the apparent resistivity measurement and then the reliability of the resistivity and the chloride profile: the instrument itself, the measurement protocol, the contact of the electrodes with the material, the type of material and its heterogeneity.

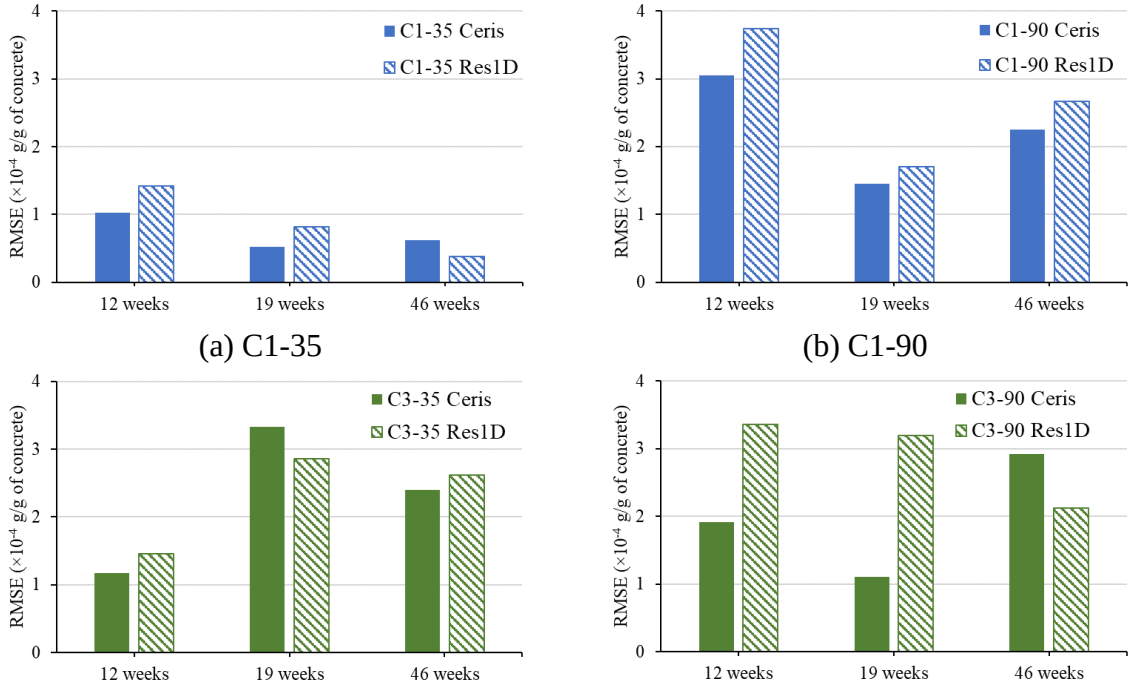

(a) C1-35 (b) C1-90

(c) C3-35 (d) C3-90

Figure 13: RMSE for free chlorides profiles obtained by DE and NDE (CERIS and Res1D)

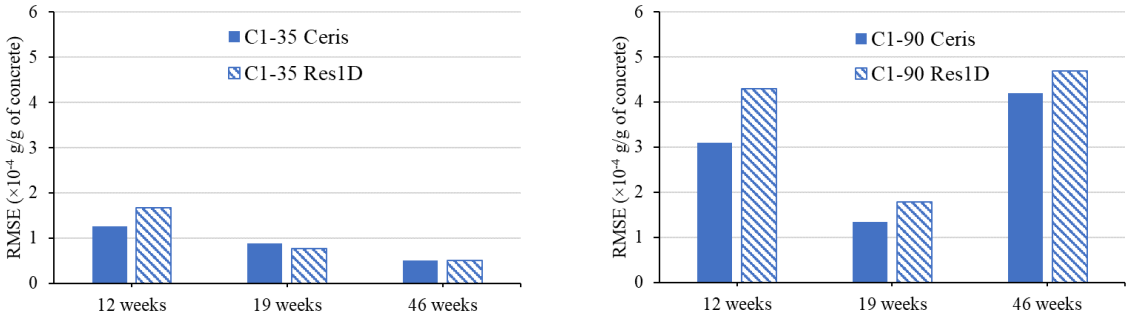

(a) C1-35 (b) C1-90

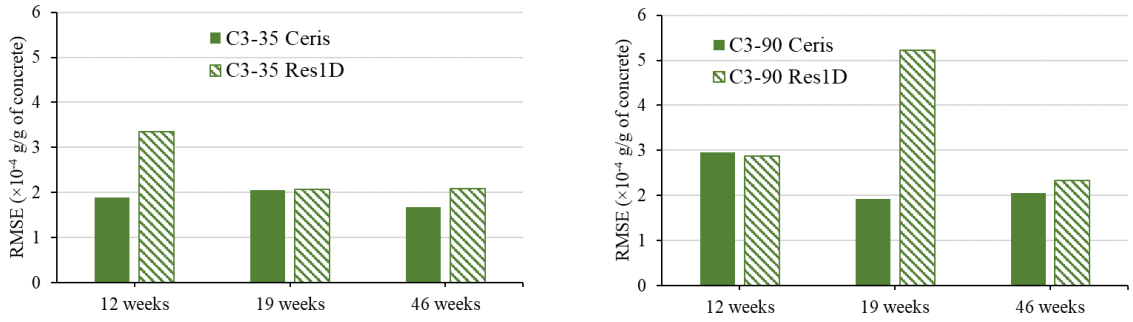

(c) C3-35 (d) C3-90

Figure 14: RMSE for total chlorides profiles obtained by DE and NDE (CERIS and Res1D)

Concerning the DE profiles, the small diameter of the core extracted from the slab (5 cm) at 12 and 19 weeks, compared to the maximum diameter of the coarse aggregate (2.2 cm), can affect negatively the reliability of the destructive profiles. Thus, at certain depths, the concrete powder obtained by grinding does not represent the real chloride concentration located in the cement paste on the same depth of the whole slab. Therefore, we chose a larger diameter (9 cm) for the extracted core at the last diffusion time '46 weeks', where we can remark a small improvement in the similarity between the DE and NDE chloride profiles especially for concrete C3 (see Figure 14). Moreover, the different steps of the destructive protocol used to determine chloride profile could affect the reliability of the chloride content: grinding, powder recovery, chloride extraction, and dilution and concentration measurements. In addition, it is possible that bound chlorides could be released during water-soluble ions extraction, which results an overestimating of free chloride content and an underestimating for total chloride content.

Despite all these sources of uncertainty, the similarity between the DE and NDE profiles highlights the ability of the NDE methodology to monitor the evolution of chloride diffusion even for concrete with very high resistivity such concrete C3.

5. Conclusion

In this paper, the monitoring of free and total chloride content profiles using a NDE methodology during a diffusion campaign was carried out on two concretes (with and without slag) of 6 years old. The methodology is based on determining the electrical resistivity profiles by carrying out surface apparent resistivity measurements submitted to two different inversion processes. The resistivity profiles are then converted to chlorides profiles using calibration curves. The NDE profiles were also compared by those assessed by DE at three different exposure periods**.** Many conclusions could be determined based on the results of this campaign:

- The increase of the electrical resistivity of concrete C3 at 6 years of curing compared to that obtained at 90 days was explained by the refinement of the microstructure (MIP results) due to the bridging of the gaps between cement particles thanks to the latent hydraulic effect of BFS,
- The increase of the electrical resistivity of concrete C3 was also explained by the decreasing of the electrical conductivity and the pH of the pore solution due to the high consuming of portlandite during the pozzolanic reaction of BFS,
- The free and total chloride profiles obtained either by DE and NDE for the two sodium chloride concentrations show the positive effect of BFS by improving the chloride resistance of concrete. The improvement was deduced by obtaining steep profiles for concrete C3, where chlorides ions were agglomerated near to the external surface whereas they were spread homogeneously along the slabs of concrete C1.
- The comparison of the chloride profiles obtained by DE and NDE displays a very good similarity which is demonstrated by the small RMSE values obtained even for mature BFS concrete (C3) with high electrical resistivity,
- The use of a new inversion method 'CERIS' was improving the reliability of the resistivity inversed profiles by reducing the difference between the DE and NDE chloride profiles due to the realistic resistivity profile shape obtained with CERIS,

In future work, the chloride profiles obtained by NDE will be used to calculate durability indicators such as the apparent diffusion coefficient and the surface chloride concentration which are used for prediction. The NDE methodology used in this work could be applied to auscultate in-situ structures after its validation on laboratory specimens, in order reduce the time-consuming of DE experiments.

Funding Acknowledgements

The authors would like to thank MAST-LAMES laboratory of Université Gustave Eiffel and GeM laboratory of Nantes University for their contribution to the experimental campaign.

6. References

[1] Eurocode 2, CEN - EN 1992-1-1 - Eurocode 2: Design of concrete structures - Part 1-1: General rules and rules for buildings_Engineering360, (1992). https://standards.globalspec.com/std/9934829/EN%201992-1-1.

[2] M. Collepardi, A. Marcialis, R. Turriziani, Penetration of Chloride Ions into Cement Pastes and Concretes, Journal of the American Ceramic Society. 55 (1972) 534–535. https://doi.org/10.1111/j.1151-2916.1972.tb13424.x.

[3] J. Crank, The mathematics of diffusion, Oxford University Press, Ely House, London W.I. SECOND EDITION (1975) 421.

[4] K. Tuutti, Corrosion of steel in concrete, Swedish Cement and Concrete Research Institute, Lund University. (1982) 473.

[5] U. Angst, B. Elsener, C. Larsen, Ø. Vennesland, Critical chloride content in reinforced concrete — A review, Cement and Concrete Research. 39 (2009) 1122–1138. https://doi.org/10.1016/j.cemconres.2009.08.006.

[6] V. Baroghel-Bouny, K. Kinomura, M. Thiery, S. Moscardelli, Easy assessment of durability indicators for service life prediction or quality control of concretes with high volumes of supplementary cementitious materials, Cement and Concrete Composites. 33 (2011) 832–847. https://doi.org/10.1016/j.cemconcomp.2011.04.007.

[7] S.E. Chidiac, D.K. Panesar, H. Zibara, The effect of short duration NaCl exposure on the surface pore structure of concrete containing GGBFS, Mater Struct. 45 (2012) 1245–1258. https://doi.org/10.1617/s11527-012-9831-4.

[8] X. Shi, N. Xie, K. Fortune, J. Gong, Durability of steel reinforced concrete in chloride environments: An overview, Construction and Building Materials. 30 (2012) 125–138. https://doi.org/10.1016/j.conbuildmat.2011.12.038.

[9] S.E. Chidiac, M. Shafikhani, Electrical resistivity model for quantifying concrete chloride diffusion coefficient, Cement and Concrete Composites. 113 (2020) 103707. https://doi.org/10.1016/j.cemconcomp.2020.103707.

[10] K.M. Rahla, R. Mateus, L. Bragança, Comparative sustainability assessment of binary blended concretes using Supplementary Cementitious Materials (SCMs) and Ordinary Portland Cement (OPC), Journal of Cleaner Production. 220 (2019) 445–459. https://doi.org/10.1016/j.jclepro.2019.02.010.

[11] G.J. Osborne, Durability of Portland blast-furnace slag cement concrete, Cement and Concrete Composites. 21 (1999) 11–21. https://doi.org/10.1016/S0958-9465(98)00032-8.

[12] A. Ben Fraj, S. Bonnet, A. Khelidj, New approach for coupled chloride/moisture transport in non-saturated concrete with and without slag, Construction and Building Materials. 35 (2012) 761–771. https://doi.org/10.1016/j.conbuildmat.2012.04.106.

[13] M. Maes, E. Gruyaert, N.D. Belie, Resistance of concrete with blast-furnace slag against chlorides, investigated by comparing chloride profiles after migration and diffusion, Materials and Structures. 46 (2013) 89–103. https://doi.org/10.1617/s11527-012-9885-3.

[14] P. Duan, Z. Shui, W. Chen, C. Shen, Enhancing microstructure and durability of concrete from ground granulated blast furnace slag and metakaolin as cement replacement materials, Journal of Materials Research and Technology. 2 (2013) 52–59. https://doi.org/10.1016/j.jmrt.2013.03.010.

[15] S. Teng, T.Y.D. Lim, B.S. Divsholi, Durability and mechanical properties of high strength concrete incorporating ultra fine Ground Granulated Blast-furnace Slag, Construction and Building Materials. 40 (2013) 875–881. https://doi.org/10.1016/j.conbuildmat.2012.11.052.

[16] J. Zhang, Y. Ma, J. Zheng, J. Hu, J. Fu, Z. Zhang, H. Wang, Chloride diffusion in alkali-activated fly ash/slag concretes: Role of slag content, water/binder ratio, alkali content and sand-aggregate ratio, Construction and Building Materials. 261 (2020) 119940. https://doi.org/10.1016/j.conbuildmat.2020.119940.

[17] W. Chen, H. Zhu, Z. He, L. Yang, L. Zhao, C. Wen, Experimental investigation on chloride-ion penetration resistance of slag containing fiber-reinforced concrete under drying-wetting cycles, Construction and Building Materials. 274 (2021) 121829. https://doi.org/10.1016/j.conbuildmat.2020.121829.

[18] C.Z. Li, Xi.B. Song, L. Jiang, A time-dependent chloride diffusion model for predicting initial corrosion time of reinforced concrete with slag addition, Cement and Concrete Research. 145 (2021) 106455. https://doi.org/10.1016/j.cemconres.2021.106455.

[19] B. Touil, F. Ghomari, A. Khelidj, S. Bonnet, O. Amiri, Durability assessment of the oldest concrete structure in the Mediterranean coastline: The Ghazaouet harbour, Marine Structures. 81 (2022) 103121. https://doi.org/10.1016/j.marstruc.2021.103121.

[20] M. Saleem, M. Shameem, S.E. Hussain, M. Maslehuddin, Effect of moisture, chloride and sulphate contamination on the electrical resistivity of Portland cement concrete, Construction and Building Materials. 10 (1996) 209–214. https://doi.org/10.1016/0950-0618(95)00078-X.

[21] G. Villain, A. Ihamouten, R. du Plooy, S.P. Lopes, X. Dérobert, Use of electromagnetic non-destructive techniques for monitoring water and chloride ingress into concrete, Near Surface Geophysics. 13 (2015) 299–309. https://doi.org/10.3997/1873-0604.2015016.

[22] Y. Lecieux, F. Schoefs, S. Bonnet, T. Lecieux, S. Palma Lopes, Quantification and uncertainty analysis of a structural monitoring device: detection of chloride in concrete using DC electrical resistivity measurement, Nondestructive Testing and Evaluation. 30 (2015) 216–232. https://doi.org/10.1080/10589759.2015.1029476.

[23] M. Fares, G. Villain, S. Bonnet, S. Palma Lopes, Determining chloride content profiles in concrete using an Electrical Resistivity Tomography device, Cement and Concrete Composites. 94 (2018) 315–326. https://doi.org/10.1016/j.cemconcomp.2018.08.001.

[24] C.E.T. Balestra, T.A. Reichert, W.A. Pansera, G. Savaris, Evaluation of chloride ion penetration through concrete surface electrical resistivity of field naturally degraded structures present in marine environment, Construction and Building Materials. 230 (2020) 116979. https://doi.org/10.1016/j.conbuildmat.2019.116979.

[25] D.S. Shevtsov, I.D. Zartsyn, E.S. Komarova, Relation between resistivity of concrete and corrosion rate of reinforcing bars caused by galvanic cells in the presence of chloride, Cement and Concrete Composites. 119 (2021) 104026. https://doi.org/10.1016/j.cemconcomp.2021.104026.

[26] M.H. Loke, Electrical imaging surveys for environmental and engineering studies. A practical guide to 2-D and 3-D surveys, RES2DINV Manual. IRIS Instruments. (2000) www.iris-intruments.com.

[27] W. Morris, A. Vico, M. Vazquez, S.R. DeSanchez, Corrosion of reinforcing steel evaluated by means of concrete resistivity measurements, Corros Sci. 44 (2002) 81–89. https://doi.org/10.1016/S0010-938X(01)00033-6.

[28] L. Marescot, S. Rigobert, S. Palma Lopes, R. Lagabrielle, D. Chapellier, A general approach for DC apparent resistivity evaluation on arbitrarily shaped 3D structures, Journal of Applied Geophysics. 60 (2006) 55–67. https://doi.org/10.1016/j.jappgeo.2005.12.003.

[29] Y. Fargier, G. Villain, S. Palma Lopes, M. Fares, Optimized retrieval of 1D-resistivity profiles in cover concrete by electrical sounding measurements, Journal of Applied Geophysics. (2021) 104413. https://doi.org/10.1016/j.jappgeo.2021.104413.

[30] B.S. Divsholi, L. Lim T.Y.D., S. Teng, Durability Properties and Microstructure of Ground Granulated Blast Furnace Slag Cement Concrete, Int J Concr Struct Mater. 8 (2014) 157–164. https://doi.org/10.1007/s40069-013-0063-y.

[31] A. Elahi, P.A.M. Basheer, S.V. Nanukuttan, Q.U.Z. Khan, Mechanical and durability properties of high performance concretes containing supplementary cementitious materials, Construction and Building Materials. 24 (2010) 292–299. https://doi.org/10.1016/j.conbuildmat.2009.08.045.

[32] A. Lübeck, A.L.G. Gastaldini, D.S. Barin, H.C. Siqueira, Compressive strength and electrical properties of concrete with white Portland cement and blast-furnace slag, Cement and Concrete Composites. 34 (2012) 392–399. https://doi.org/10.1016/j.cemconcomp.2011.11.017.

[33] R.A. Medeiros-Junior, M.G. Lima, Electrical resistivity of unsaturated concrete using different types of cement, Construction and Building Materials. 107 (2016) 11–16. https://doi.org/10.1016/j.conbuildmat.2015.12.168.

[34] R. Du Plooy, S. Palma Lopes, G. Villain, X. Dérobert, Development of a multi-ring resistivity cell and multi-electrode resistivity probe for investigation of cover concrete condition, NDT & E International. 54 (2013) 27–36. https://doi.org/10.1016/j.ndteint.2012.11.007.

[35] A.R. Chini, L.C. Muszynski, J. Hicks, Determination of Acceptance Permeability Characteristics for Performance-Related Specifications for Portland Cement Concrete, Florida Department of Transportation (Contract No. BC 354-41). (2003) 165.

[36] M.A. Alhajj, S. Palma-Lopes, G. Villain, Accounting for steel rebar effect on resistivity profiles in view of reinforced concrete structure survey, Construction and Building Materials. 223 (2019) 898–909. https://doi.org/10.1016/j.conbuildmat.2019.07.208.

[37] R. Du Plooy, G. Villain, S. Palma Lopes, A. Ihamouten, X. Dérobert, B. Thauvin, Electromagnetic non-destructive evaluation techniques for the monitoring of water and chloride ingress into concrete: a comparative study, Mater Struct. 48 (2015) 369–386. https://doi.org/10.1617/s11527-013-0189-z.

[38] F. Wenner, A method for measuring earth resistivity, Journal of the Washington Academy of 531 Sciences. 5 (1915) 561–563.

[39] L. Marescot, S. Rigobert, S.P. Lopes, R. Lagabrielle, D. Chapellier, A general approach for DC apparent resistivity evaluation on arbitrarily shaped 3D structures, Journal of Applied Geophysics. 1 (2006) 55–67. https://doi.org/10.1016/j.jappgeo.2005.12.003.

[40] M.A. Alhajj, S. Bourguignon, S. Palma Lopes, G. Villain, Joint inversion of electromagnetic measurements for the determination of water saturation profiles in concrete structures, Cement and Concrete Research. 147 (2021) 106500. https://doi.org/10.1016/j.cemconres.2021.106500.

[41] R. Du Plooy, The developement and combiantion of electromagnetic non-destructive evaluation techniques for the assessement of cover concrete condition prior to corrosion, Thèse de doctorat, Université de Nantes, 2013.

[42] M.H. Loke, Tutorial : 2-D and 3-D electrical imaging surveys, (2015) 187.

[43] K. Levenberg, A method for the solution of certain non-linear problems in least square, Quarterly of Applied Mathematics. 2 (1944) 164–168.

[44] D.W. Marquardt, An Algorithm for Least-Squares Estimation of Nonlinear Parameters, Journal of the Society for Industrial and Applied Mathematics. 11 (1963) 431–441.

[45] M. Fares, Y. Fargier, G. Villain, X. Derobert, S. Palma Lopes, Determining the permittivity profile inside reinforced concrete using capacitive probes, NDT & E International. 79 (2016) 150–161. https://doi.org/10.1016/j.ndteint.2016.01.002.

[46] A.M. Neville, J.J. Brooks, Concrete technology, Pearson Education Limited. Second Edition (2010) 460.

[47] J. Kuziak, P. Woyciechowski, R. Kobyłka, A. Wcisło, The content of chlorides in blast-furnace slag cement as a factor affecting the diffusion of chloride ions in concrete, MATEC Web Conf. 163 (2018) 05007. https://doi.org/10.1051/matecconf/201816305007.

[48] G. Arliguie, H. Hornain, GranDuBé – Grandeurs associées à la durabilité des bétons (durability-related parameters_in French), RGCU–AFGC–Presses de l'ENPC, Paris. (2007) 63–106.

[49] NT BUILD 492, Concrete, Mortar and Cement-based repair materials: chloride migration coefficient from non-steady-state migration experiments, (1999).

[50] Q. Zhou, F.P. Glasser, Thermal stability and decomposition mechanisms of ettringite at <120°C, Cement and Concrete Research. 31 (2001) 1333–1339. https://doi.org/10.1016/S0008-8846(01)00558-0.

[51] A. Fabien, M. Choinska, S. Bonnet, A. Pertue, A. Khelidj, Aggregate size effects on the mechanical behaviour and on the gas permeability at damaged state of cement-based materials with and without slag, European Journal of Environmental and Civil Engineering. 0 (2021) 1–22. https://doi.org/10.1080/19648189.2021.1915881.

[52] R.T. 178-TMC, Analysis of water soluble chloride content in concrete,Recommendation, Materials and Structures. 35 (2002) 586–588.

[53] R. Cherif, A.A. Hamami, A. Aït-Mokhtar, J.-F. Meusnier, Study of the pore solution and the microstructure of mineral additions blended cement pastes, Energy Procedia. 139 (2017) 584–589. https://doi.org/10.1016/j.egypro.2017.11.257.

[54] O. Vennesland, M.-A. Climent, C. Andrade, Recommendation of RILEM TC 178-TM.Testing and modelling chloride penetration in concret. Methods for obtaining dust samples by means of grinding concrete in order to determine the chloride concentration profile, (2013) 12. https://doi.org/10.1617/s11527-012-9968-1.

[55] T. Chaussadent, G. Arliguie, AFREM test procedures concerning chlorides in concrete: Extraction and titration methods, Mat. Struct. 32 (1999) 230–234. https://doi.org/10.1007/BF02481520.

[56] W. Morris, E.I. Moreno, A.A. Sagüés, Practical evaluation of resistivity of concrete in test cylinders using a Wenner array probe, Cement and Concrete Research. 26 (1996) 1779–1787. https://doi.org/10.1016/S0008-8846(96)00175-5.

[57] L.O. Nilsson, M.H. Ngo, O.E. Gjørv, High-performance repair materials for concrete structures in the port of Gothenburg, in: Second International Conference on Concrete under Severe Conditions: Environment and Loading, Spon, London, 1998: pp. 1193–1198.

[58] L. Shen, Z. Chen, Critical review of the impact of tortuosity on diffusion, Chemical Engineering Science. 62 (2007) 3748–3755. https://doi.org/10.1016/j.ces.2007.03.041.

[59] L. Rui, C. Yuebo, W. Changyi, H. Xiaoming, Study of chloride binding and diffusion in GGBS concrete, Cement and Concrete Research. 33 (2003) 7.

[60] C. Arya, N.R. Buenfeld, J.B. Newman, Factors influencing chloride-binding in concrete, Cement and Concrete Research. 20 (1990) 291–300. https://doi.org/10.1016/0008-8846(90)90083-A.

[61] P. Spiesz, M.M. Ballari, H.J.H. Brouwers, RCM: A new model accounting for the non-linear chloride binding isotherm and the non-equilibrium conditions between the free- and bound-chloride concentrations, Construction and Building Materials. 27 (2012) 293–304. https://doi.org/10.1016/j.conbuildmat.2011.07.045.

[62] C.-L. Page, Diffusion of chloride ions in hardened cement pastes, Cement and Concrete Research. 11 (1981) 395–406.

[63] A. Younsi, Ph. Turcry, A. Aït-Mokhtar, S. Staquet, Accelerated carbonation of concrete with high content of mineral additions: Effect of interactions between hydration and drying, Cement and Concrete Research. 43 (2013) 25–33. https://doi.org/10.1016/j.cemconres.2012.10.008.

[64] R. Cherif, A.E.A. Hamami, A. Aït-Mokhtar, Global quantitative monitoring of the ion exchange balance in a chloride migration test on cementitious materials with mineral additions, Cement and Concrete Research. 138 (2020) 106240. https://doi.org/10.1016/j.cemconres.2020.106240.

[65] A. Lübeck, A.L.G. Gastaldini, D.S. Barin, H.C. Siqueira, Compressive strength and electrical properties of concrete with white Portland cement and blast-furnace slag, Cement and Concrete Composites. 34 (2012) 392–399. https://doi.org/10.1016/j.cemconcomp.2011.11.017.

[66] Y. Liu, Accelerated curing of concrete with high volume Pozzolans-resistivity, diffusivity and compressive strength, Ph.D., 2012. https://www.proquest.com/docview/1315747772/abstract/D7B0404470A041D2PQ/1 (accessed May 23, 2023).

[67] R.B. Polder, Test methods for on site measurement of resistivity of concrete - a RILEM TC-154 technical recommendation, 15 (2001) 125–131.

[68] F. Hunkeler, The resistivity of pore water solution—a decisive parameter of rebar corrosion and repair methods, Construction and Building Materials. 10 (1996) 381–389. https://doi.org/10.1016/0950-0618(95)00029-1.

[69] Z.M. Sbartaï, S. Laurens, J. Rhazi, J.P. Balayssac, G. Arliguie, Using radar direct wave for concrete condition assessment: Correlation with electrical resistivity, Journal of Applied Geophysics. 4 (2007) 361–374. https://doi.org/10.1016/j.jappgeo.2007.02.003.

[70] G.E. Archie, The Electrical Resistivity Log as an Aid in Determining Some Reservoir Characteristics, Transactions of the AIME. 146 (1942) 54–62. https://doi.org/10.2118/942054-G.

[71] C. Shi, X. Hu, X. Wang, Z. Wu, G. Schutter, Effects of Chloride Ion Binding on Microstructure of Cement Pastes, J. Mater. Civ. Eng. 29 (2017) 04016183. https://doi.org/10.1061/(ASCE)MT.1943-5533.0001707.

[72] M. Castellote, M.C. Alonso, C. Andrade, Standardization, to a reference of 25 °C, of electrical resistivity for mortars and concretes in saturated or isolated conditions, ACI Materials Journal. 99 (2002) 119–127.

[73] Y. Liu, F. Presuel, Effect of Elevated Temperature Curing on Compressive Strength and Electrical Resistivity of Concrete with Fly Ash and GGBS, MJ. 111 (2014) 531–542. https://doi.org/10.14359/51686913.

[74] J. Badr, E. Mahfoud, G. Villain, J.-P. Balayssac, S. Palma Lopes, Y. Fargier, B. Yven, Temperature Effect on Electrical Resistivity Measurement Using an Embedded Sensor to Estimate Concrete Water Content, Applied Sciences. 12 (2022) 9420. https://doi.org/10.3390/app12199420.

[75] R. Cai, Y. Hu, M. Yu, W. Liao, L. Yang, A. Kumar, H. Ma, Skin effect of chloride ingress in marine concrete: A review on the convection zone, Construction and Building Materials. 262 (2020) 120566. https://doi.org/10.1016/j.conbuildmat.2020.120566.

[76] M. Shakouri, D. Trejo, A study of the factors affecting the surface chloride maximum phenomenon in submerged concrete samples, Cement and Concrete Composites. 94 (2018) 181–190. https://doi.org/10.1016/j.cemconcomp.2018.09.006.

[77] L.P. Tang, 9178489482 Chloride Ingress in Concrete Exposed to Marine Environment: Field Data Up to 10 Years Exposure, SP Swedish National Testing and Research Institute, Sweden, 2003. - Google Search, (n.d.). https://www.google.com/search?client=firefox-b-d&q=L.P.+Tang%2C+9178489482+Chloride+Ingress+in+Concrete+Exposed+to+Marine+Environment%3A+Field+Data+Up+to+10+Years+Exposure%2C+SP+Swedish+National+Testing+and+Research+Institute%2C+Sweden%2C+2003. (accessed May 22, 2023).

[78] A. Lindvall, Chloride ingress data from field and laboratory exposure – Influence of salinity and temperature, Cement and Concrete Composites. 29 (2007) 88–93. https://doi.org/10.1016/j.cemconcomp.2006.08.004.

[79] T. Luping, Engineering expression of the ClinConc model for prediction of free and total chloride ingress in submerged marine concrete, Cement and Concrete Research. 38 (2008) 1092–1097. https://doi.org/10.1016/j.cemconres.2008.03.008.

[80] S. Bonnet, F. Schoefs, M. Salta, Sources of uncertainties for total chloride profile measurements in concrete: quantization and impact on probability assessment of corrosion initiation, European Journal of Environmental and Civil Engineering. 24 (2017) 232–247. https://doi.org/10.1080/19648189.2017.1375997.